

ÇANKAYA UNIVERSITY  
GRADUATE SCHOOL OF NATURAL AND APPLIED SCIENCES  
ELECTRONIC AND COMMUNICATION ENGINEERING

MASTER THESIS

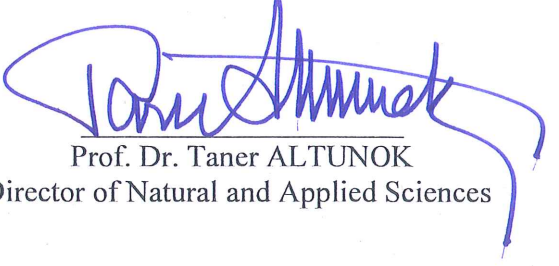
WIRELESS OPTICAL WAVE PROPAGATION IN UNDERWATER MEDIUM

AYSAN KESKİN


SEPTEMBER 2013

Title of Thesis : **Wireless Optical Wave Propagation in Underwater Medium**  
Submitted by **Aysan KESKİN**

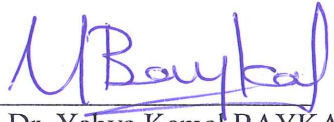
Approval of the Graduate School of Natural and Applied Sciences:

  
Prof. Dr. Taner ALTUNOK  
Director of Natural and Applied Sciences

I certify that this thesis satisfies all the requirements as a thesis for the degree of Master of Science.

  
Prof. Dr. Celal Zaim ÇİL  
Chairman of Electronic and  
Communication Engineering

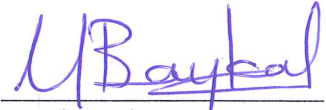
This is to certify that we have read this thesis and that in our opinion it is fully adequate, in scope and quality, as a thesis for the degree of Master of Science.

  
Prof. Dr. Yahya Kemal BAYKAL  
Supervisor

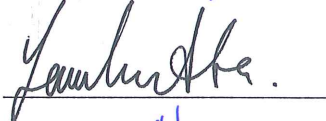
**Thesis Examining Date:** 05.09.2013

**Examining Committee Members:**

Prof. Dr. Yahya Kemal BAYKAL (Çankaya Univ.)



Dr. Yalçın ATA (TÜBİTAK SAGE)



Yrd. Doç. Dr. Serap Altay ARPALI (Çankaya Univ.)



## STATEMENT OF NON-PLAGIARISM

I hereby declare that all information in this document has been obtained and presented in accordance with academic rules and ethical conduct. I also declare that, as required by these rules and conduct, I have fully cited and referenced all material and results that are not original to this work.

Name, Last name : Aysan KESKİN

Date : 05.09.2013

Signature :



## **ABSTRACT**

### **WIRELESS OPTICAL WAVE PROPAGATION IN UNDERWATER MEDIUM**

KESKİN, Aysan

M. Sc., Department of Electronic and Communication Engineering

Supervisor: Prof. Dr. Yahya Kemal BAYKAL

September 2013, 58 pages

In this thesis, the effects of the turbulence on the average transmittance are examined when the lowest order collimated Gaussian optical beam wave propagates in a wireless underwater medium. To observe the oceanic turbulence effect, the power spectrum of homogeneous and isotropic oceanic water combining the effects of salinity and temperature is used. Employing the Rytov method and the numeric integration, the effects of the parameters of power spectrum on the average transmittance are analyzed. Obtaining results with the help of Matlab program indicates that the rate of dissipation of the kinetic energy per unit mass of fluid is directly proportional to the average transmittance while the rate of dissipation of the mean-squared temperature is inversely proportional to the average transmittance. Increase in the link distance and decrease in the wavelength reduce the average transmittance. When the temperature-induced optical turbulence is dominant in the ratio of the salinity and temperature contributions to the refractive index spectrum, the average transmittance almost never decreases. However, the salinity-induced

optical turbulence reduces the average transmittance sharply. Increasing the Kolmogorov microscale length, first the turbulence effect increases and the average transmittance decreases, but when the value of Kolmogorov microscale is further increased, the turbulence effect starts to decrease and the average transmittance increases, eventually a saturation is observed.

**Keywords:** Underwater Optics, Underwater Turbulence, Optical Wave Propagation, Optical Wireless Communications

## ÖZ

### SUALTI ORTAMINDA KABLOSUZ OPTİK DALGA YAYILIMI

KESKİN, Aysan

Yüksek Lisans, Elektronik ve Haberleşme Mühendisliği

Tez Yöneticisi: Prof. Dr. Yahya Kemal BAYKAL

Eylül 2013, 58 sayfa

Bu tezde, en düşük dereceli koşutlanmış optik Gauss ışın demetinin sualtı ortamında kablosuz yayılımında oluşan ortalama geçirgenlik üzerine türbülansın etkisi incelenmiştir. Okyanustaki türbülansın etkisini gözlemlemek için, tuzluluk ve sıcaklık etkileriyle bileşen homojen ve eşyönlü okyanus suyunun güç spektrumu kullanıldı. Rytov metodu ve nümerik integrasyon kullanılarak, güç spektrumunu oluşturan parametrelerin ortalama geçirgenlik üzerine etkileri incelendi. Matlab programının yardımıyla elde edilen sonuçlara göre, ortalama geçirgenliğin ortalama karesel sıcaklık dağılım oranı ile ters orantılı, akışkanın birim kütesine düşen kinetik enerji dağılım oranı ile doğru orantılı olduğu belirlendi. Yayılım mesafesinin artması ve dalgaboyunun küçülmesi halinde ise ortalama geçirgenlik azalmaktadır. Tuzluluk ve sıcaklığın kırılma indisi spektrumuna katkısı oranının sıcaklık içerikli optik türbülans ile ifade edilen kısmı, ortalama geçirgenliği neredeyse hiç azaltmamaktadır. Fakat tuzluluk bazlı optik türbülans, ortalama geçirgenliği kesin bir şekilde düşürmektedir. Kolmogorov küçük ölçek uzunluğundaki artış, önce

türbölans etkisini arttırmakta ve ortalama geçirgenliđi azaltmakta, ancak Kolmogorov küçük ölçek uzunluđu daha fazla arttırıldıđında, türbölans etkisi düşmekte ve ortalama geçirgenlik artmakta, sonunda ise bir doyum gözlemlenmektedir.

**Anahtar Kelimeler:** Sualtı Optik, Sualtı Türbölans, Optik Dalga Yayılımı, Optik Telsiz (Kablosuz) Haberleşme

I would like to extend my deepest gratitude to the most honored Mr. M. Sadullah ÖZTÜRK, whose presence and selfless support give me strength.



## **ACKNOWLEDGMENTS**

I would like to thank to my graduate advisor, Prof. Dr. Yahya Kemal BAYKAL, for introducing me this topic and for his valuable guidance and endless help, encouragement throughout my undergraduate and graduate studies.

I offer my sincere thanks to my family for their understanding, support and values which they have taught during this study and all my life.

## TABLE OF CONTENTS

<b>STATEMENT OF NON-PLAGIARISM.....</b>	<b>iii</b>
<b>ABSTRACT.....</b>	<b>iv</b>
<b>ÖZ.....</b>	<b>vi</b>
<b>ACKNOWLEDGMENTS .....</b>	<b>ix</b>
<b>TABLE OF CONTENTS.....</b>	<b>x</b>
<b>LIST OF TABLES .....</b>	<b>xii</b>
<b>LIST OF FIGURES .....</b>	<b>xiii</b>
<b>LIST OF SYMBOLS .....</b>	<b>xvi</b>
<b>LIST OF ABBREVIATIONS .....</b>	<b>xx</b>
<b>CHAPTER 1 INTRODUCTION .....</b>	<b>1</b>
<b>CHAPTER 2 FORMULATION .....</b>	<b>13</b>
2.1 Propagation of Gaussian Beam Waves in Turbulent Underwater Medium .....	14
2.2 Turbulence Effect and the Rytov Method.....	18
2.3 The Mutual Coherence Function.....	22
2.4 The Average Intensity and the Average Transmittance.....	24
<b>CHAPTER 3 RESULTS AND VALIDATION .....</b>	<b>26</b>
3.1 Validation of the Results in Atmospheric Optics.....	27
3.2 Results on the Average Intensity in Underwater Media .....	29

3.3 Results on the Average Transmittance in Underwater Media .....	31
<b>CHAPTER 4 CONCLUSION .....</b>	<b>48</b>
4.1 Conclusion .....	48
4.2 Future Works.....	50
<b>REFERENCES.....</b>	<b>51</b>
<b>APPENDIX A SAMPLE MATLAB CODE .....</b>	<b>55</b>
<b>APPENDIX B CURRICULUM VITAE .....</b>	<b>58</b>

## LIST OF TABLES

<b>Table 1.1</b> Jerlov water types.....	4
<b>Table 1.2</b> Absorption, scattering, and attenuation coefficient values for typical water types at blue-green region.....	5

## LIST OF FIGURES

<b>Figure 1.1</b> Absorption, scattering and extinction coefficients versus wavelength for two different chlorophyll concentrations.....	6
<b>Figure 1.2</b> Absorption coefficient of chlorophyll versus wavelength for Jerlov water types.....	7
<b>Figure 1.3</b> Scattering coefficient for small and large particles versus wavelength.....	8
<b>Figure 2.1</b> (a) convergent beam, (b) collimated beam, (c) divergent beam.....	16
<b>Figure 2.2</b> Amplitude profile of Gaussian beam wave.....	17
<b>Figure 3.1</b> Intensity profile versus the link distance in the atmosphere when the extended Huygens-Fresnel principle is used.....	28
<b>Figure 3.2</b> Intensity profile versus the link distance in the atmosphere when the Rytov method is used.....	28
<b>Figure 3.3</b> Intensity profile versus distance from beam center line in the transverse direction $r$ for different link distance $L$ .....	29
<b>Figure 3.4</b> The average intensity profile versus $r$ for different beam size $\alpha_s$ .....	30
<b>Figure 3.5</b> The average transmittance versus the ratio of the salinity-temperature contributions for different $X_T$ values.....	32
<b>Figure 3.6</b> The average transmittance versus the ratio of the salinity-temperature contributions for different $\varepsilon$ values.....	33

<b>Figure 3.7</b>	The average transmittance versus the ratio of the salinity-temperature contributions for different $L$ values.....	34
<b>Figure 3.8</b>	The average transmittance versus the ratio of the salinity-temperature contributions for different $\lambda$ values.....	35
<b>Figure 3.9</b>	The average transmittance versus the rate of dissipation of the mean-squared temperature for different $\varepsilon$ values.....	36
<b>Figure 3.10</b>	The average transmittance versus the rate of dissipation of the mean-squared temperature for different $L$ values.....	37
<b>Figure 3.11</b>	The average transmittance versus the rate of the dissipation of the mean-squared temperature for different $\lambda$ values.....	38
<b>Figure 3.12</b>	The average transmittance versus the link distance for different $\varepsilon$ values.....	39
<b>Figure 3.13</b>	The average transmittance versus the link distance for different $\lambda$ values.....	40
<b>Figure 3.14</b>	The average transmittance versus the wavelength for different $\varepsilon$ values.....	41
<b>Figure 3.15</b>	The average transmittance versus Kolmogorov microscale length for different $w$ values.....	42
<b>Figure 3.16</b>	The average transmittance versus Kolmogorov microscale length for different $X_T$ values.....	43
<b>Figure 3.17</b>	The average transmittance versus Kolmogorov microscale length for different $\varepsilon$ values.....	44
<b>Figure 3.18</b>	The average transmittance versus Kolmogorov microscale length for different $L$ values.....	45

**Figure 3.19** Average transmittance versus Kolmogorov microscale length for different  $\lambda$  values.....46

## LIST OF SYMBOLS

<b>Symbols</b>	<b>Definitions</b>
$a(\lambda)$	Absorption coefficient ( $\text{m}^{-1}$ )
$b(\lambda)$	Scattering coefficient ( $\text{m}^{-1}$ )
$c(\lambda)$	Extinction coefficient ( $\text{m}^{-1}$ )
$z$	Link distance (m)
$L$	Distance (m)
$\mathbf{r}$	Position vector at receiver plane
$\mathbf{s}$	Position vector at source plane
$r$	Distance from the beam center line in the transverse direction at receiver plane (m)
$s$	Distance from the beam center line in the transverse direction at source plane (m)
$r_x$	Receiver transverse coordinate (m)
$r_y$	Receiver transverse coordinate (m)
$s_x$	Source transverse coordinate (m)
$s_y$	Source transverse coordinate (m)



<b>Symbols</b>	<b>Definitions</b>
$U_0(\mathbf{s}, 0)$	Beam field at source plane
$U_0(\mathbf{r}, z)$	Beam field at receiver plane without turbulence
$U(\mathbf{r}, L)$	Beam field at receiver plane with turbulence
$a_0$	Amplitude ( $(\text{W}/\text{m}^2)^{1/2}$ )
$\alpha_s$	Source size (m)
$F_0$	Phase front radius of curvature
$k$	Wave number
$\lambda$	Wavelength
$\alpha$	Complex parameter related to the spot size and phase front radius of curvature
$\theta$	Degree (rad)
$J_n(x)$	$n^{\text{th}}$ order Bessel function
$\Psi(\mathbf{r}, L)$	Complex phase perturbation
$\langle \rangle$	Ensemble average
*	Conjugation operator
$E_1(0, 0)$	First order moment (statistical moments of the Rytov approximation)
$\kappa$	Amplitude of the spatial frequency
$\xi$	The normalized distance variable
$\Phi_n(\kappa)$	Power spectrum

## Symbols

## Definitions

$\Lambda$	Imaginary part of non-dimensional output plane beam parameter
$\Theta$	Real part of non-dimensional output plane beam parameter
$\Theta_0$	Real part of non-dimensional input plane beam parameter
$\Lambda_0$	Imaginary part of non-dimensional input plane beam parameter
$F$	Receiver plane phase front radius of curvature (m)
$W$	Receiver plane beam radius (m)
$L_0$	Outer scale (m)
$l_0$	Inner scale (m)
$\varepsilon$	The rate of dissipation of kinetic energy per unit mass of fluid ( $\text{m}^2/\text{s}^3$ )
$\eta$	The Kolmogorov micro scale length (m)
$X_T$	The rate of dissipation of the mean-squared temperature ( $\text{K}^2/\text{s}$ )
$w$	Non-dimensional ratio of temperature and salinity contributions to the refractive index spectrum
$\Gamma_2(\mathbf{r}_1, \mathbf{r}_2, L)$	Mutual coherence function
$\Gamma_2^0(\mathbf{r}_1, \mathbf{r}_2, L)$	Mutual coherence function for free space
$I(\mathbf{r}, L)$	Received intensity with turbulence

## Symbols

## Definitions

$I^0(\mathbf{r}, L)$

Received intensity without turbulence

$\tau_t$

Transmittance normalized by the received intensity without turbulence

$\tau_s$

Transmittance normalized by the intensity at the source plane

$C_n^2$

The refractive-index structure constant in atmosphere ( $\text{m}^{-2/3}$ )

$\delta$

Function about Kolmogorov microscale and inner scale

## LIST OF ABBREVIATIONS

<b>Abbreviations</b>	<b>Definitions</b>
AUV	Autonomous underwater vehicle
ROV	Remotely operated vehicle
LED	Light emitting diode
MODTRAN	Moderate resolution atmospheric transmission
DWDM	Dense wavelength division multiplexing
TEM	Transverse electromagnetic
MCF	Mutual coherence function
BER	Bit error ratio
Matlab	A type of programming language

<b>Units</b>	<b>Definitions</b>
m	Meter
s	Second
m/s	Meter per second

<b>Units</b>	<b>Definitions</b>
km	Kilometer
cm	Centimeter
$\mu\text{m}$	Micrometer
nm	Nanometer
Gbps	Giga bit per second
Mbps	Mega bit per second
kbps	Kilo bit per second
bps	Bit per second
mg	Milligram
MHz	Mega hertz
K	Kelvin
rad	Radian

## **CHAPTER 1**

### **INTRODUCTION**

In the past few years, interest in the underwater wireless communication is increased. Most underwater wireless communication systems today utilize acoustical methods. Acoustical communication has restrictions due to its limited data bit rate. Acoustic waves transmit data at low carrier frequency and travel at low speed. While the speed of sound is approximately 340 m/s in air, in underwater medium such as sea, it is about 1500m/s [1]. In acoustical communications, energy is highly consumed and large antennas are used. Data can be transmitted to long range; however, latency is very high. High latency is a problem for real time response, synchronization, and multiple access protocols. In deep ocean, data transmission rates are about 20 kbps within up to one kilometer and 300-500 bps within up to 200 km. In shallow water, 300-500 bps transmission rates can be obtained up to 100 km [2]. Therefore, acoustical method does not satisfy the emerging applications. To overcome these disadvantages of the acoustical communications, an alternative which is the wireless optical communication in underwater medium is becoming popular.

Optical wave propagation consumes low energy and can form a cost-effective alternative to acoustical communications in underwater medium. Electromagnetic

waves having a speed of 300.000.000 m/s in vacuum are somewhat slower in underwater, are much faster than acoustic waves. Propagation of light waves is effected by the temperature, salinity, depth and various constituents of water. As the result, the optical waves are highly attenuated in water so they cannot travel very far in underwater medium. However, the use of optical waves brings the advantage of high data rate transmission in underwater medium [1][2][3][4].

In the past few years, the amount of scientific research about underwater is increased in the areas of defense, transportation, detection of water pollution, sensor networks and the related industries. In some detail, these fields cover the underwater sensor network and observatories, security and harbor inspections, surveying and oil rings and pipelines, autonomous underwater vehicle (AUV) communication, remotely operated vehicle (ROV) telemetry and telecommand. Most of these applications profit from the high data transmission rate advantage of the optical communication which are in the range of 1Mbps to 1Gbps, high fidelity of data transmission, conservative power budget, low cost and reproducibility [4].

Investigating optical wireless communication systems in underwater environment is quite a difficult task owing to the nature of water. Light is highly exposed to distorting effects of water. Some of these factors are the water types, absorption, scattering, temperature, salinity, chlorophyll concentration, optical clarity and turbulence. Effect of the water types is a crucial parameter for wireless communication in underwater environment. Absorption and scattering are the two main processes affecting the light propagation in underwater medium. Other

parameters like the temperature and salinity affect the light propagation which is elaborated below in this chapter and in chapter 4.

### ***Water Types***

Water clarity changes dramatically from one location to another due to the organic and inorganic materials and sediments involved in water. Living organisms existing in rivers, lakes and oceans cause discrepancies to concentration of the water. Characteristics of water can make difference depending on where it is situated in the world. The oceanographic community has studied for decades to classify the types of water. Water clarity and color was classified by Jerlov in the 1950s [5]. This classification that appears in the literature as the Jerlov water types is given in Table 1.1. In the literature four major water types are discussed which are classified as the pure sea water, clear ocean water, coastal ocean water and the turbid harbor water [5][6][7][8]. In pure sea water, the main limiting factor is the absorption and in short distances the beam propagation is in straight lines because of the small scattering coefficient and forward scattering angle. Clear ocean water includes dissolved particles which cause scattering. In coastal ocean water, the problems are both scattering and absorption since the concentration of water has a large amount of mineral components and planktonic matters. Turbid harbor water has highest concentration of dissolved matters.



**Table 1.1** Jerlov water types.

<b>Jerlov Water Types</b>	<b>Classification of Water</b>
Type I	Clearest ocean waters
Type IA and Type IB	These types has clarity between Type I and Type II, Type IA is clearer than Type IB
Type II	Intermediate waters
Type III	Murkiest waters
C1 to C9 (Coastal 1 to Coastal 9)	More turbid coastal waters (C1 is clearest water and C9 is least clear)

### ***Absorption and Scattering***

One of the main causes of attenuation is the absorption which originates from the inorganic materials like water molecules, dissolved salts and organic substances such as chlorophyll and coloured dissolved organic matters. Scattering, which is deviation of the photons from true path, is the other main factor that affects the propagation of light in underwater medium. Light propagation is much sensitive to wavelength since both absorption and scattering depend on the wavelength of operation. Absorption and scattering coefficient defined as  $a(\lambda)$  and  $b(\lambda)$ , respectively constitute the total attenuation coefficient. Total attenuation coefficient is defined by the extinction coefficient  $c(\lambda)$  which is defined below in Equation 1.1 [2][8].

$$c(\lambda) = a(\lambda) + b(\lambda) \tag{1.1}$$

In different water types, these coefficients show an alteration as seen in Table 1.2 [6][7][9][10].

**Table 1.2** Absorption, scattering, and attenuation coefficient values for typical water types at blue-green region.

<b>Water Type</b>	<b><math>a(\lambda)</math> [<math>\text{m}^{-1}</math>]</b>	<b><math>b(\lambda)</math> [<math>\text{m}^{-1}</math>]</b>	<b><math>c(\lambda)</math> [<math>\text{m}^{-1}</math>]</b>
Pure sea water	0.0405	0.0025	0.043
Clean ocean	0.114	0.037	0.151
Coastal ocean	0.179	0.219	0.298
Turbid harbor	0.266	1.824	2.19

Especially in pure seawater, scattering and absorption are affected by the suspended particulate matters. In absorption, energy changes occur, however, in scattering there is no change in the energy. In pure sea water, active content increasing the attenuation is the dissolved salt ions. In different water types such as lakes and river, chlorophyll concentration and coloured dissolved organic matters raise the attenuation. For two different chlorophyll concentrations, the absorption, scattering, and the total attenuation coefficient (extinction coefficient) variations over the wavelength from 400 nm to 700 nm are given in Figure 1.1 [8].

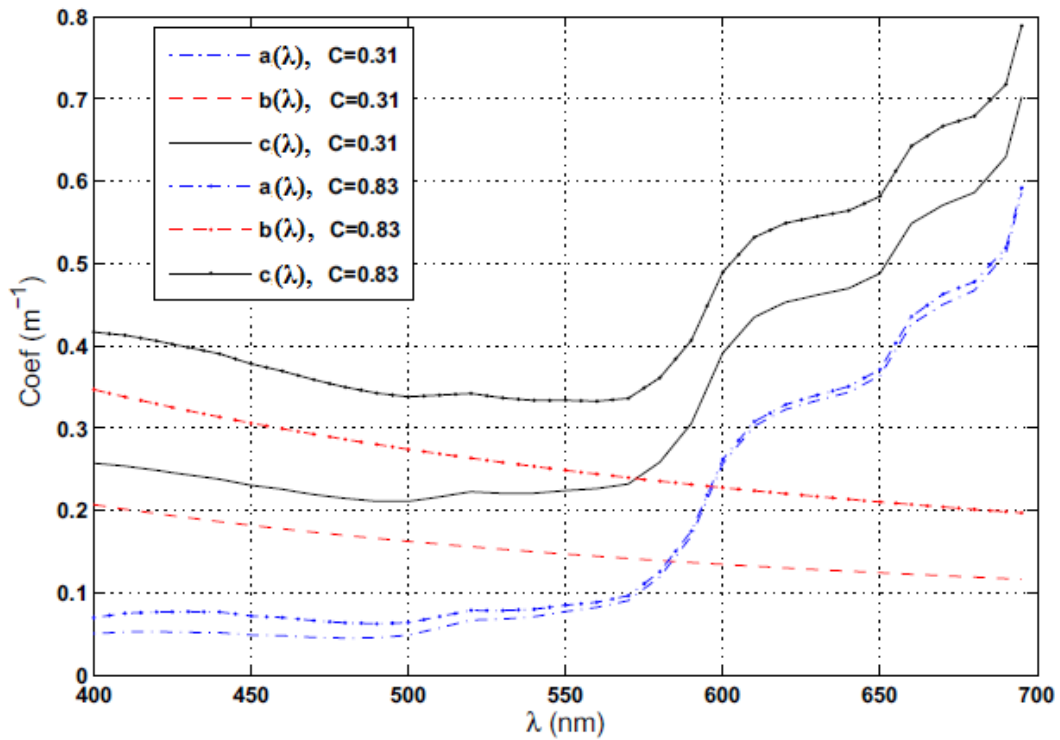


**Figure 1.1** Absorption, scattering and extinction coefficients versus wavelength for two different chlorophyll concentrations.

Here  $C$  represents the chlorophyll concentrations. When the chlorophyll concentration increases, we see that both the absorption and the scattering coefficients has become larger. Moreover we can see that the appropriate wavelength range is the blue-green region according to the extinction coefficient for light propagation in underwater medium. If chlorophyll concentration is discussed in detail as a function of wavelength for different water types, blue-green region is again convenient, which can be seen in Figure 1.2 [11]. Having different chlorophyll concentration, if the absorption coefficient of the chlorophyll is analyzed with respect to wavelength in Jerlov water types, the absorbance goes on increasing from clearest water type I to murkiest water coastal 2.

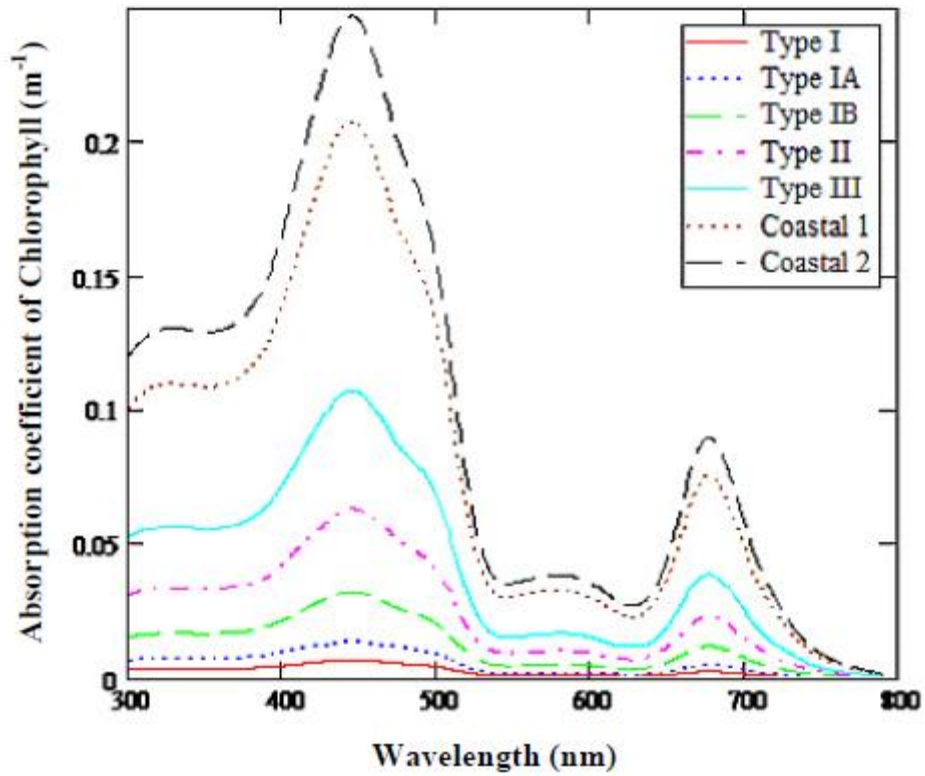


**Figure 1.2** Absorption coefficient of chlorophyll versus wavelength for Jerlov water types.

Scattering also depends on the size of the particles. The angle of scattering is dependent on the size of the particles so the direction of propagation changes. The scattering coefficient of small and large particles versus the wavelength is shown in Figure 1.3 [12].

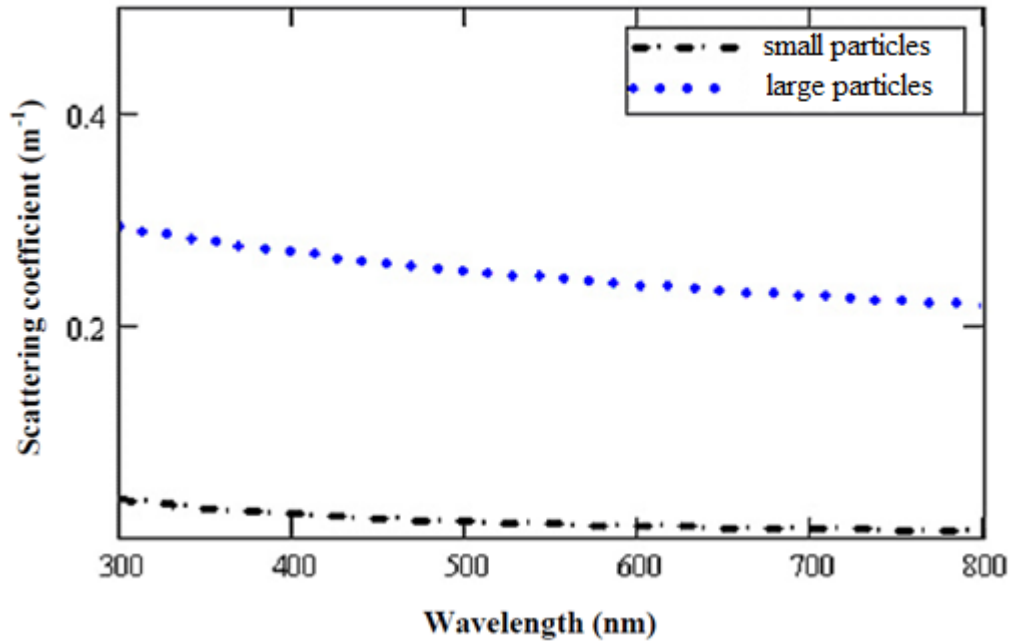


**Figure 1.3** Scattering coefficient for small and large particles versus wavelength.

The temperature and the salinity are also very important parameters that affect light propagation in the underwater. The crucial effect of the fluctuations in the temperature and the salinity is the turbulence effect in water which degrades the optical signal as it propagates under the water. Light propagation in oceanic turbulence is more difficult to formulate when compared to formulation of atmospheric turbulence because of the complexity of underwater environment. Turbulence has been studied for around hundred years, but its characteristic has not been completely solved yet in classical physics. Analyses in turbulence generally are simplified using three basic assumptions for flow statistics [13]. These are

- Stationary (invariant with respect to translation in time)
- Homogeneous (invariant with respect to translation in space)
- Isotropic (invariant with respect to rotations)

Under these assumptions, the evaluations are usually made by focusing on the power spectra that defines the turbulence effect in the water. In this thesis, for homogeneous and isotropic ocean, water power spectrum which includes the thermal diffusivity and the diffusion of salt is used. The power spectrum will be discussed in detail in chapter 2.

Being a very challenging field, there exists some studies on the light propagation in underwater environment. These works are more related to the intensity profiles and the underwater turbulence structure. The current transmission data rates employed in the wireless optical communication in underwater medium are not adequate to meet the needs of the demanding technology. In recent years, theoretical and experimental studies have been done, but this field still needs to be enhanced. Further research is necessary to find methods to overcome the absorption, scattering and degradation in the received signal in order to increase the transmittance over longer link distances and to achieve higher data bit rates. Some of the researches executed up to now are mentioned in the following part of this paragraph. In 1995, Bales and Chryssostomidis studied LED based wireless underwater optical communication theoretically. They obtained results that 10 Mbps and 1 Mbps data could be transmitted 20 m and 30 m, respectively [14]. In 2005, Giles and Bankman calculated the transmission distances for 220 kbps and 4.4 Mbps data rates and they found the ranges altering from 10 m to 25 m [15]. Farr et al claimed that 10 MHz transmission through 100 m is possible in omni-directional LED communication system in 2006 [16]. Hanson and Radic, using laser instead of LED, provided 1 Gbps data rate in 2 m pipe experimentally in 2007 [7]. In the same year, Jim Simpson used

LED and photodetector instead of laser and photomultiplier tubes. He obtained high data rate transmission (1-100 Mbps) at relatively short ranges (<100 m) [4]. In 2008, Arnon and Kedar indicated that the wireless underwater sensor networks provide high data rate for mobile users for a distance of up to 100 m [2]. In 2010, Heather Brundage designed an optical communication system using LED. He achieved that data could be transmitted by 1 Mbps over distances of 13 m without much loss [1]. Shchepakina, Farwell, and Korotkova used the optical source which is Gaussian-Shell model with initial Gaussian spectral profile in turbulent ocean and they found that the link distance can be self-reconstructed in relatively short distances [17]. In the same year again Korotkova and Farwell examined the intensity and the coherence characteristics of Gaussian beam and saw the effect of optical turbulence on the intensity [18].

There are a few studies in literature about optical transmittance and light transmission in underwater environment. Among these work, the experimental study done by H. J. Okoomian in 1966 is referred to in which the characteristics of the transmission of visual radiation in water is examined and the transmission data range is expanded with intense pulses of laser radiation [19]. In 1986, Pierce et al. reported the transmittance of the solar radiation into and through the water column of the Rhode River estuary. They explained the spectral changes and energy losses through the water column as a function of changes in water quality parameters [20]. Nowadays, Nicolaus et al. published a paper which covers variability of light transmission through Arctic land-fast sea ice. Their results show that partial snow melt causes increase in the light transmittance. Moreover, light transmittance is time-

invariant and differences were directly related to the variability of snow cover. It is observed that snow cover variability constitutes the transmittance seasons. The first one is prior to onset of melt. In this season, the spatial variability did not change with time. In the second, the relative spatial variability was constant into the melt season. In the third one, seasonal increase in transmittance before melt is much larger than the relative spatial variability in either period [21]. Regarding the transmittance in atmospheric optics, in 2003, Baykal found the average transmittance using a partially coherent source. He obtained the correct average intensity for coherent, partially coherent and incoherent sources, then found the average transmittance due to turbulence for practical free space optics communication links [22]. In 2011, Ata and Baykal analyzed the effect of atmospheric turbulence on the atmospheric optics telecommunication links using Dense Wavelength Division Multiplexing (DWDM). They obtained the transmittance with MODerate resolution atmospheric TRANsmission (MODTRAN) code for partially coherent sources. Turbulence is found to be the determining factor of transmittance for long distance links. In DWDM systems, coherent sources reduce the MODTRAN transmittance more than the partially coherent sources. In long distance DWDM systems with turbulent atmosphere, MODTRAN transmittance is found to be reduced at any DWDM wavelength and at any source coherence [23].

Most of the studies in wireless underwater communication are related to underwater sensor networks. Up to now, in the literature, there are a few studies for finding the turbulence effects when optical waves propagate in an underwater medium [17][18]. In this thesis, the underwater turbulence effect on the optical transmittance is



investigated. Parameters which constitute the power spectrum of turbulence and the effects of these parameters on the transmittance are discussed in detail in this study.

## CHAPTER 2

### FORMULATION

In this chapter, the methodology, specific formulas and the calculation used in the thesis are presented. When preparing the thesis, the author is inspired by the free space and atmospheric optics because of the similarity of light propagation and its formulation in the atmosphere and in underwater. Naturally, there are some differences such as the medium characteristics and the energy spectra.

In this thesis, the effect of oceanic turbulence on the average transmittance is analyzed using Rytov method and mutual coherence function (MCF). The lowest order collimated Gaussian beam is chosen as the optical source. First, the propagation of the beam is examined in free space, i.e., in the absence of water turbulence. In section 2.1, Gaussian beam is defined at the source plane. For link distance  $z=L$  (horizontal link) the received field is calculated with no turbulence using the Huygens-Fresnel integral which is introduced from Equation 2.1 to 2.10. Then in section 2.2, the water turbulence effect is calculated and introduced into the beam propagation in free space with Rytov method that is in Equation 2.11. The effects due to oceanic turbulence are determined by the power spectrum. This power spectrum, which is valid for the homogeneous and isotropic oceanic water with the eddy thermal diffusivity and diffusion of salt, is introduced in Equation

2.21. Numerical integration method is used in the evaluations. After finding the turbulence effect of ocean using Rytov method, to find the average intensity, Mutual Coherence Function (MCF) is defined in section 2.3. For special condition of MCF which is  $\mathbf{r}_1 = \mathbf{r}_2 = \mathbf{r}$ , the average intensity can be found from the mutual coherence function where  $\mathbf{r}_1$  and  $\mathbf{r}_2$  are the points at the receiver plane. Finally, in section 2.4, the average intensity formulation and calculation are given and then the average transmittance is found by normalizing the average intensities.

### 2.1 Propagation of Gaussian Beam Waves in Turbulent Underwater Medium

Gaussian beam, which manifest clearly the characteristics of an optical beam, is an important solution of the paraxial Helmholtz equation. The intensity distribution of Gaussian function is symmetrically centered about the beam axis in any transverse plane, the beam power is all around the beam axis, when the beam width decreases, the beam waist increases in both directions. Many types of lasers radiate light in Gaussian wave form [24]. Gaussian beam is also named as the lowest order mode, called TEM<sub>00</sub> wave. Gaussian beam wave function at the transverse plane  $z = 0$ , also called the source plane, is given in Equation 2.1 [25].

$$U_0(s, 0) = a_0 \exp\left(-\frac{s^2}{2\alpha_s^2} - \frac{iks^2}{2F_0}\right) \quad (2.1)$$

This equation can be written in a different form as seen below:

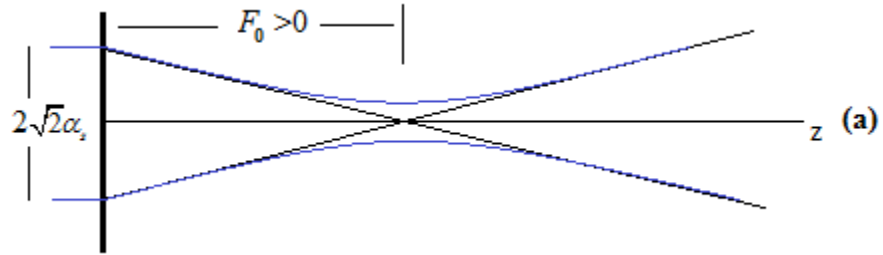
$$U_0(\mathbf{s}, 0) = a_0 \exp\left(-\frac{1}{2}\alpha k |\mathbf{s}|^2\right) \quad (2.2)$$

where

$$\alpha = \frac{1}{k\alpha_s^2} + \frac{i}{F_0} \quad (2.3)$$

is the complex parameter related to the spot size and phase front radius of curvature,  $\mathbf{s}$  is the source transverse coordinate,  $a_0$  is the amplitude in  $(\text{W}/\text{m}^2)^{1/2}$ ,  $s = |\mathbf{s}| = (s_x^2 + s_y^2)^{1/2}$  is the distance from the beam center line in the transverse direction at source plane in m (at receiver plane the transverse coordinate is shown by  $\mathbf{r}$ ),  $\alpha_s$  is the source size in m,  $k = \frac{2\pi}{\lambda}$  is the wave number in  $\text{m}^{-1}$ ,  $\lambda$  is the wavelength,  $F_0$  is the radius of curvature in m.

According to the radius of curvature, three types of beams which are the convergent beam  $F_0 > 0$ , the collimated beam  $F_0 = \infty$ , and the divergent beam  $F_0 < 0$  are identified and is seen in Figure 2.1 schematically [25].



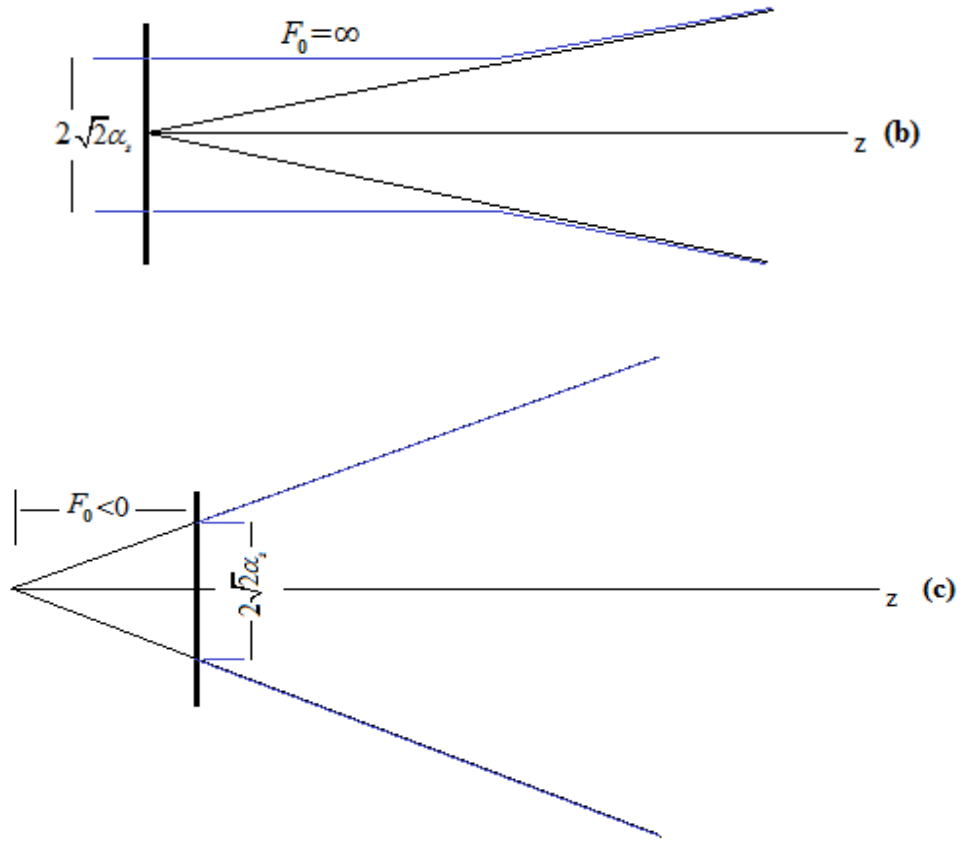


**Figure 2.1** (a) convergent beam, (b) collimated beam, (c) divergent beam.

Amplitude profile of the field of the first order mode, i.e., the Gaussian beam is plotted using Matlab program for the source size  $\alpha_s = 0.71$  cm and the phase front radius of curvature  $F_0 = \infty$  in Figure 2.2.

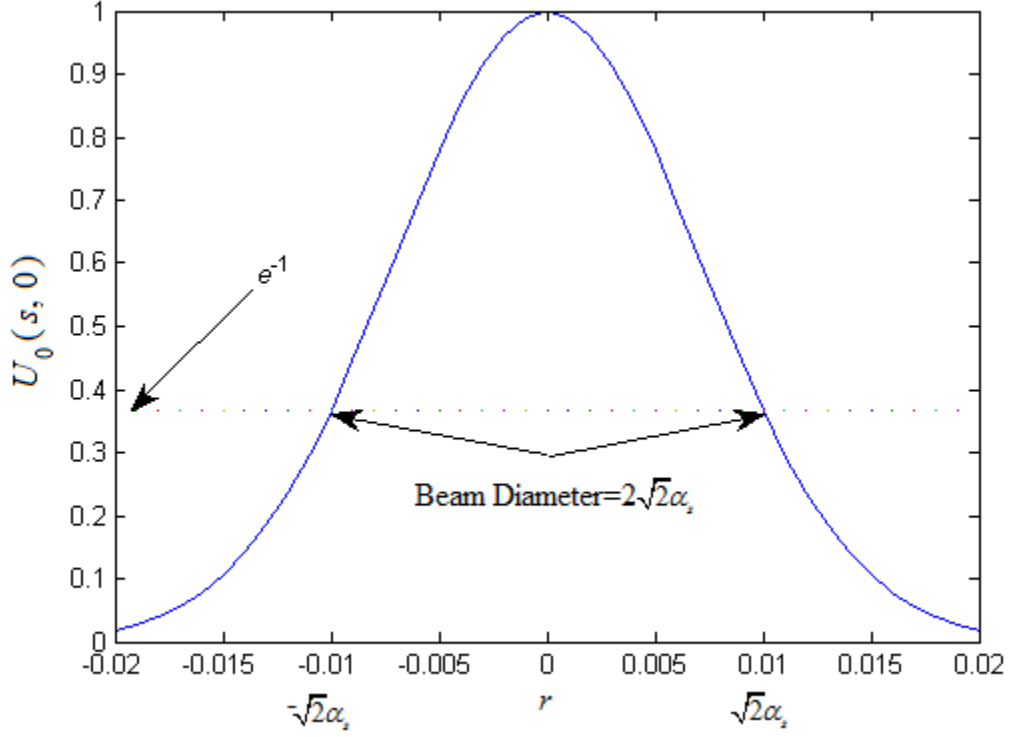


**Figure 2.2** Amplitude profile of Gaussian beam wave.

Since the Rytov method is used in this thesis, first the propagation of Gaussian beam in free space at the receiver distance  $z = L$ , in other words Gaussian beam wave at the receiver plane ( $z = L$ ) without turbulence is found. Here  $L$  is defined as the link distance. Taking  $a_0 = 1$  and using the Huygens-Fresnel principle, the field at the receiver plane is found to be [25].

$$\begin{aligned}
 U_0(\mathbf{r}, z) = & -\frac{ik}{2\pi z} \exp\left(ikz + \frac{ik}{2z}|\mathbf{r}|^2\right) \\
 & \times \int_{-\infty}^{\infty} \int_{-\infty}^{\infty} \exp\left(-\frac{ik}{z}\mathbf{r}\cdot\mathbf{s}\right) \exp\left[\frac{ik}{2z}(1+i\alpha z)|\mathbf{s}|^2\right] d^2\mathbf{s}
 \end{aligned} \tag{2.4}$$

Converting to polar coordinates

$$\begin{aligned}
U_0(r, z) = & -\frac{ik}{2\pi z} \exp\left(ikz + \frac{ik}{2z} r^2\right) \\
& \times \int_0^\infty \int_0^{2\pi} \exp\left(-\frac{ik}{z} rs \cos \theta\right) \exp\left[\frac{ik}{2z}(1+i\alpha z)s^2\right] s d\theta ds
\end{aligned} \tag{2.5}$$

where  $r = |\mathbf{r}| = (r_x^2 + r_y^2)^{1/2}$  is the distance from the beam center line in the transverse direction at receiver plane.

For the integration over  $\theta$ , the equation

$$\int_0^{2\pi} \exp\left(-\frac{ik}{z} rs \cos \theta\right) d\theta = 2\pi J_0(krs/z) \tag{2.6}$$

is used where  $J_0(x)$  is the first kind and zero order Bessel function [26] which is

$$\begin{aligned}
J_n(x) &= \sum_{k=0}^{\infty} \frac{(-1)^k \left(\frac{x}{2}\right)^{2k+n}}{k!(k+n)!} & -\infty < x < \infty \\
J_0(x) &= \sum_{k=0}^{\infty} \frac{(-1)^k \left(\frac{x}{2}\right)^{2k}}{k!^2}
\end{aligned} \tag{2.7}$$

Inserting Equation 2.6 into Equation 2.5

$$\begin{aligned}
U_0(r, z) = & -\frac{ik}{z} \exp\left(ikz + \frac{ik}{2z} r^2\right) \\
& \times \int_0^\infty s J_0(krs/z) \exp\left[\frac{ik}{2z}(1+i\alpha z)s^2\right] ds
\end{aligned} \tag{2.8}$$

Integrating Equation 2.8 with respect to s, we obtain

$$U_0(r, z) = \frac{1}{1+i\alpha z} \exp\left[ikz + \frac{ik}{2z} \left(\frac{i\alpha z}{1+i\alpha z}\right) r^2\right] \tag{2.9}$$

At the link distance  $L$ , i.e., when  $z=L$ ,

$$U_0(r, L) = \frac{1}{1+i\alpha L} \exp\left[ikL + \frac{ik}{2L} \left(\frac{i\alpha L}{1+i\alpha L}\right) r^2\right] \tag{2.10}$$

## 2.2 Turbulence Effect and the Rytov Method

The Rytov method formulation is given by Equation 2.11. This equation shows that the received field is obtained by the product of the field in the absence of turbulent and the field due to turbulence. Thus, the received is expressed as [25].

$$\begin{aligned}
 U(\mathbf{r}, L) &= U_0(\mathbf{r}, L) \exp[\Psi(\mathbf{r}, L)] \\
 &= U_0(\mathbf{r}, L) \exp[\Psi_1(\mathbf{r}, L) + \Psi_2(\mathbf{r}, L) + \dots]
 \end{aligned} \tag{2.11}$$

where  $\exp[\Psi(\mathbf{r}, L)]$  represents the field due to turbulence,  $\Psi(\mathbf{r}, L)$  is the total complex phase perturbation of the field,  $\Psi_1(\mathbf{r}, L)$  is the first order complex phase perturbation,  $\Psi_2(\mathbf{r}, L)$  is the second order complex phase perturbation. Since in the average intensity and the average transmittance formulations,  $\langle \exp[\Psi(\mathbf{r}, L)] \rangle$  and  $\langle \exp[\Psi(\mathbf{r}_1, L) + \Psi^*(\mathbf{r}_2, L)] \rangle$  terms are required where  $\langle \rangle$  represents the ensemble average, these terms are expressed below [25].

$$\langle \exp[\Psi(\mathbf{r}, L)] \rangle = \langle \exp[\Psi_1(\mathbf{r}, L) + \Psi_2(\mathbf{r}, L)] \rangle \tag{2.12}$$

$$\begin{aligned}
 \langle \exp[\Psi(\mathbf{r}_1, L) + \Psi^*(\mathbf{r}_2, L)] \rangle &= \langle \exp[\Psi_1(\mathbf{r}_1, L) + \Psi_2(\mathbf{r}_1, L) \\
 &\quad + \Psi_1^*(\mathbf{r}_2, L) + \Psi_2^*(\mathbf{r}_2, L)] \rangle
 \end{aligned} \tag{2.13}$$

Introducing the center of gravity and the difference vectors which are

$$\mathbf{r} = \frac{1}{2}(\mathbf{r}_1 + \mathbf{r}_2), \quad \mathbf{p} = \mathbf{r}_1 - \mathbf{r}_2$$

$$r = |\mathbf{r}|, \quad \rho = |\mathbf{p}|$$



First order and second order moments (in Equation 2.12) with second order complex phase quantities are given below[25]

$$E_1(0,0) = \langle \Psi_2(\mathbf{r}, L) \rangle + \frac{1}{2} \langle \Psi_1^2(\mathbf{r}, L) \rangle$$

$$E_2(\mathbf{r}_1, \mathbf{r}_2) = \langle \Psi_1(\mathbf{r}_1, L) \Psi_1^*(\mathbf{r}_2, L) \rangle \quad (2.14)$$

The ensemble averages are given below [25].

$$\langle \exp[\Psi(\mathbf{r}, L)] \rangle = \exp[E_1(0,0)] \quad (2.15)$$

$$\langle \exp[\Psi(\mathbf{r}_1, L) + \Psi^*(\mathbf{r}_2, L)] \rangle = \exp[2E_1(0,0) + E_2(\mathbf{r}_1, \mathbf{r}_2)] \quad (2.16)$$

where  $E_1(0,0)$  and  $E_2(\mathbf{r}_1, \mathbf{r}_2)$  are the parameters including the power spectrum, hence the effect of oceanic turbulence is introduced in this part. Mathematical expressions are provided below [25].

$$E_1(0,0) = -2\pi^2 k^2 L \int_0^\infty \kappa \Phi_n(\kappa) d\kappa \quad (2.17)$$

$$E_2(\mathbf{r}_1, \mathbf{r}_2) = 4\pi^2 k^2 L \times \int_0^1 \int_0^\infty \kappa \Phi_n(\kappa) J_0 \left[ \kappa \left| (1 - \bar{\Theta} \xi) \mathbf{p} - 2i\Lambda \xi \mathbf{r} \right| \right] \exp \left( -\frac{\Lambda L \kappa^2 \xi^2}{k} \right) d\kappa d\xi \quad (2.18)$$

where  $\kappa$  is the amplitude of the spatial frequency which is scalar ( $2\pi/L_0 < \kappa < 2\pi/l_0$ ),  $L_0$  and  $l_0$  denote the outer scale and inner scale, respectively,  $\Phi_n(\kappa)$  is the power spectrum,  $\xi$  is the normalized distance variable ( $0 \leq \xi \leq 1$ ),  $\bar{\Theta}$  and  $\Lambda$  are non-dimensional output plane beam parameters whose definitions are [25].

$$\Theta = 1 + \frac{L}{F} = \frac{\Theta_0}{\Theta_0^2 + \Lambda_0^2}$$

$$\bar{\Theta} = -\frac{L}{F} = 1 - \Theta$$

$$\Lambda = \frac{2L}{kW^2} = \frac{\Lambda_0}{\Theta_0^2 + \Lambda_0^2} \quad (2.19)$$

where

$$\Theta_0 = 1 - \frac{L}{F_0}, \quad \Lambda_0 = \frac{2L}{k(\sqrt{2}\alpha_s)^2} \quad (2.20)$$

where  $F_0$  and  $\alpha_s$  denote the source plane phase front radius of curvature and the source size,  $F$  and  $W$  denote the receiver plane phase front radius of curvature and beam radius.

The most important entity in these equations is the power spectrum  $\Phi_n(\kappa)$  which includes the eddy thermal diffusivity and diffusion of the salt for homogeneous and isotropic oceanic water. The eddy coefficient of thermal diffusivity and diffusion of salt should be equal to one, which can be defined  $\theta = 1$ . The power spectrum is expressed as [17][18][27].

$$\Phi_n(\kappa) = 0.388 \times 10^{-8} \varepsilon^{-1/3} \kappa^{-11/3} \left[ 1 + 2.35(\kappa\eta)^{2/3} \right]$$

$$\times \frac{X_T}{w^2} \left( w^2 e^{-A_T \delta} + e^{-A_S \delta} - 2w e^{-A_{TS}} \right) \quad (2.21)$$

where

$$\delta = 8.284(\kappa\eta)^{4/3} + 12.978(\kappa\eta)^2 \quad (2.22)$$

$\varepsilon$  is the rate of dissipation of kinetic energy per unit mass of fluid in  $\text{m}^2/\text{s}^3$ ,  $\eta$  is the Kolmogorov micro scale length in m,  $X_T$  is the rate of dissipation of the mean-squared temperature in  $\text{K}^2/\text{s}$ ,  $w$  is the unitless ratio of temperature and salinity contributions to the refractive index spectrum,  $A_T = 1.863 \times 10^{-2}$ ,  $A_S = 1.9 \times 10^{-4}$ ,  $A_{TS} = 9.41 \times 10^{-3}$  are constants.  $X_T$  has a value ranging from  $10^{-4} \frac{\text{K}^2}{\text{s}}$  to  $10^{-10} \frac{\text{K}^2}{\text{s}}$ ,  $\varepsilon$  ranges from  $10^{-1} \frac{\text{m}^2}{\text{s}^3}$  to  $10^{-10} \frac{\text{m}^2}{\text{s}^3}$ . In oceanic water, defined interval of  $w$  is  $[-5, 0]$ . If  $w$  is equal to or close to  $-5$ , the temperature-induced optical turbulence dominates. If  $w$  is about  $0$ , the salinity-induced optical turbulence dominates.

### 2.3 The Mutual Coherence Function

The mutual coherence function (MCF) [25] which is the second-order moment is defined by the ensemble average as

$$\Gamma_2(\mathbf{r}_1, \mathbf{r}_2, L) = \langle U(\mathbf{r}_1, L) U^*(\mathbf{r}_2, L) \rangle \quad (2.23)$$

where  $*$  is the conjugation operator.

Under the weak fluctuation theory, MCF is

$$\begin{aligned} \Gamma_2(\mathbf{r}_1, \mathbf{r}_2, L) &= U_0(\mathbf{r}_1, L) U_0^*(\mathbf{r}_2, L) \langle \exp[\Psi(\mathbf{r}_1, L) + \Psi^*(\mathbf{r}_2, L)] \rangle \\ &= \Gamma_2^0(\mathbf{r}_1, \mathbf{r}_2, L) \exp[2E_1(0, 0) + E_2(\mathbf{r}_1, \mathbf{r}_2)] \end{aligned} \quad (2.24)$$

Inserting Equation 2.10, the free space MCF given below is obtained.

$$\Gamma_2^0(\mathbf{r}_1, \mathbf{r}_2, L) = U_0(\mathbf{r}_1, L)U_0^*(\mathbf{r}_2, L) \quad (2.25)$$

Using Equation 2.17 and Equation 2.18 we obtain

$$\begin{aligned} \exp[2E_1(0,0) + E_2(\mathbf{r}_1, \mathbf{r}_2)] &= \exp\left(-4\pi^2 k^2 L \int_0^1 \int_0^\infty d\kappa d\xi \kappa \Phi_n(\kappa)\right. \\ &\quad \left. \times \left\{1 - \exp\left(-\frac{\Lambda L \kappa^2 \xi^2}{k}\right) J_0\left[\kappa\left|(1 - \bar{\Theta}\xi)\mathbf{p} - 2i\Lambda\xi\mathbf{r}\right|\right]\right\}\right) \end{aligned} \quad (2.26)$$

Inserting Equation 2.21 into 2.26 we obtain

$$\begin{aligned} \exp[2E_1(0,0) + E_2(\mathbf{r}_1, \mathbf{r}_2)] &= \exp\left(-4\pi^2 k^2 L \int_0^1 \int_0^\infty \kappa \left\{0.388 \times 10^{-8} \varepsilon^{-1/3} \kappa^{-11/3} \left[1 + 2.35(\kappa\eta)^{2/3}\right]\right\}\right. \\ &\quad \times \frac{X_T}{w^2} \left(w^2 e^{-A_r \delta} + e^{-A_s \delta} - 2w e^{-A_T \delta}\right) \\ &\quad \left. \times \left\{1 - \exp\left(-\frac{\Lambda L \kappa^2 \xi^2}{k}\right) J_0\left[\kappa\left|(1 - \bar{\Theta}\xi)\mathbf{p} - 2i\Lambda\xi\mathbf{r}\right|\right]\right\} d\kappa d\xi\right) \end{aligned} \quad (2.27)$$

To our knowledge, the integrals in Equation 2.27 cannot be solved analytically so we have employed the numerical integration. The method of numerical integration which is written by a Matlab program is provided by Emre Sermtulu. [28]. In our evaluations, we have chosen to examine the on axis average transmittances so  $\mathbf{p}$  and  $\mathbf{r}$  are taken to be zero. The argument of the zero order Bessel function is zero, thus the value of the Bessel part of Equation 2.27 is equal to one. Finally, MCF takes the specific form used in this thesis study which is given as

$$\begin{aligned} \Gamma_2(\mathbf{r}_1, \mathbf{r}_2, L) &= U_0(\mathbf{r}_1, L)U_0^*(\mathbf{r}_2, L) \exp\left(-4\pi^2 k^2 L \int_0^1 \int_0^\infty \kappa \Phi_n(\kappa)\right. \\ &\quad \left. \times \left\{1 - \exp\left(-\frac{\Lambda L \kappa^2 \xi^2}{k}\right) J_0\left[\kappa\left|(1 - \bar{\Theta}\xi)\mathbf{p} - 2i\Lambda\xi\mathbf{r}\right|\right]\right\}\right) d\kappa d\xi \end{aligned} \quad (2.28)$$

## 2.4 The Average Intensity and the Average Transmittance

The average intensity or the mean intensity at the receiver plane can be found by evaluating the MCF at the identical observation points  $\mathbf{r}_1 = \mathbf{r}_2 = \mathbf{r}$  at receiver plane [25].

$$\langle I(\mathbf{r}, L) \rangle = \Gamma_2(\mathbf{r}, \mathbf{r}, L) \quad (2.29)$$

There are two definitions to find the average transmittance. In the first definition, the average intensity at the receiver plane with turbulence is normalized with the average intensity at receiver plane without turbulence. In the second definition, the average intensity at the receiver plane with turbulence is divided by the average intensity at the source plane. The average transmittances within the above definitions are mathematically written as [22][24][25][29].

$$I^0(\mathbf{r}, L) = \Gamma_2^0(\mathbf{r}, \mathbf{r}, L) = U_0(\mathbf{r}, L)U_0^*(\mathbf{r}, L) \quad (2.30)$$

Here  $I^0(\mathbf{r}, z = L)$  is the intensity at the receiver plane when there is no turbulence

$$I(\mathbf{r}, z = 0) = \Gamma_2(\mathbf{r}, \mathbf{r}, 0) = U(\mathbf{r}, z = 0)U^*(\mathbf{r}, z = 0) \quad (2.31)$$

where  $I(\mathbf{r}, z = 0)$  is the average intensity at the source plane.

The average transmittance normalized by the received intensity without turbulence is

$$\langle \tau_t \rangle = \frac{\langle I(\mathbf{r}, L) \rangle}{I^0(\mathbf{r}, L)} \quad (2.32)$$

The average transmittance normalized by the intensity at the source plane is

$$\langle \tau_s \rangle = \frac{\langle I(\mathbf{r}, L) \rangle}{I(\mathbf{r}, z = 0)} \quad (2.33)$$

The average transmittance profiles are evaluated mainly by using Equation 2.32 and the results are given in following chapter. The results using Equation 2.33 are quite similar to the ones obtained by using Equation 2.32.

## CHAPTER 3

### RESULTS AND VALIDATION

The collimated Gaussian beam that has the lowest order was chosen to discover the transmittance profiles in underwater environment by using the Rytov method and mutual coherence function (MCF). The results obtained are compared to the results obtained by the extended Huygens-Fresnel integral for the atmospheric optics in section 3.1. Then, in section 3.2, the average intensity profile in underwater medium is compared to the results of appearing in the literature [18]. The average transmittance is calculated for parameters constituting the oceanic turbulence within their different values of the defined range. The default values used throughout the study and some different values for other conditions are described as follows. For the collimated Gaussian beam, the phase front radius of curvature is taken as  $F_0 = \infty$ , the source size is taken as  $\alpha_s = 0.71$  cm. The distance from the beam center  $r$  ranging from 0 to 0.02 m is defined for intensity profile to compare the results. However, in this thesis, the transmittances are evaluated at  $r=0$ . The link distance  $L$  and the wavelength  $\lambda$  are experimented for different values. The other parameters and their values are mentioned in sections 3.1 and 3.2.

### 3.1 Validation of the Results in Atmospheric Optics

In this section, the check of our results is explained to be sure of their validity. At first, Matlab program [30] was used for the Kolmogorov turbulence theory (in Equation 3.2) in atmosphere by solving the extended Huygens-Fresnel principle (in Equation 3.1[31]) which is

$$U(\mathbf{r}, L) = -\frac{ik}{2\pi L} \exp(ikL) \iint_{-\infty}^{\infty} d^2s U_0(\mathbf{s}, 0) \exp\left[\frac{ik|\mathbf{s}-\mathbf{r}|^2}{2L} + \Psi(\mathbf{r}, \mathbf{s})\right] \quad (3.1)$$

where  $U_0(\mathbf{s}, 0)$  is the optical wave at the transmitter, and  $\Psi(\mathbf{r}, \mathbf{s})$  is the random part of the complex phase of a spherical wave.

Then, a different Matlab code according to Equation 2.28 is prepared to compare with Kamacıoğlu's results [30]. In the comparison, the wavelength  $\lambda = 1.55 \mu\text{m}$ , source size  $\alpha_s = 2 \times 10^{-2} \text{ m}$ , and the structure constant  $C_n^2 = 2 \times 10^{-15} \text{ m}^{-2/3}$  were assumed.  $C_n^2$  determines the turbulence effect which takes part in the Kolmogorov theory of turbulence whose power spectrum is given as [25][31].

$$\Phi_n(\kappa) = 0.033 C_n^2 \kappa^{-11/3} \quad (3.2)$$

$C_n^2 = 0$  means that there is no turbulence in the medium.  $C_n^2 = 10^{-17} \text{ m}^{-2/3}$  expresses the weak turbulence and  $C_n^2 = 10^{-13} \text{ m}^{-2/3}$  points out the strong turbulence in atmosphere [30]. The comparisons of our numerical method results and the analytical method results in turbulent atmosphere using the extended Huygens-Fresnel principle results are provided in Figure 3.1 and Figure 3.2 in which  $C_n^2 = 10^{-15} \text{ m}^{-2/3}$  is taken. The figures with the measured data are given below.



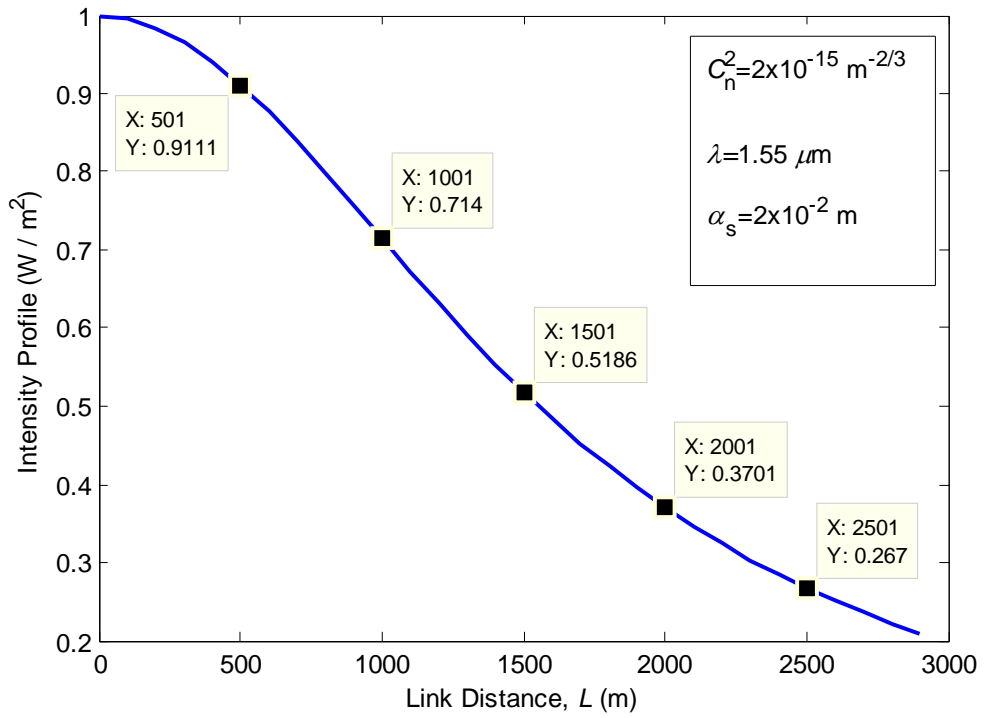


**Figure 3.1** Intensity profile versus the link distance in the atmosphere when the extended Huygens-Fresnel principle is used.

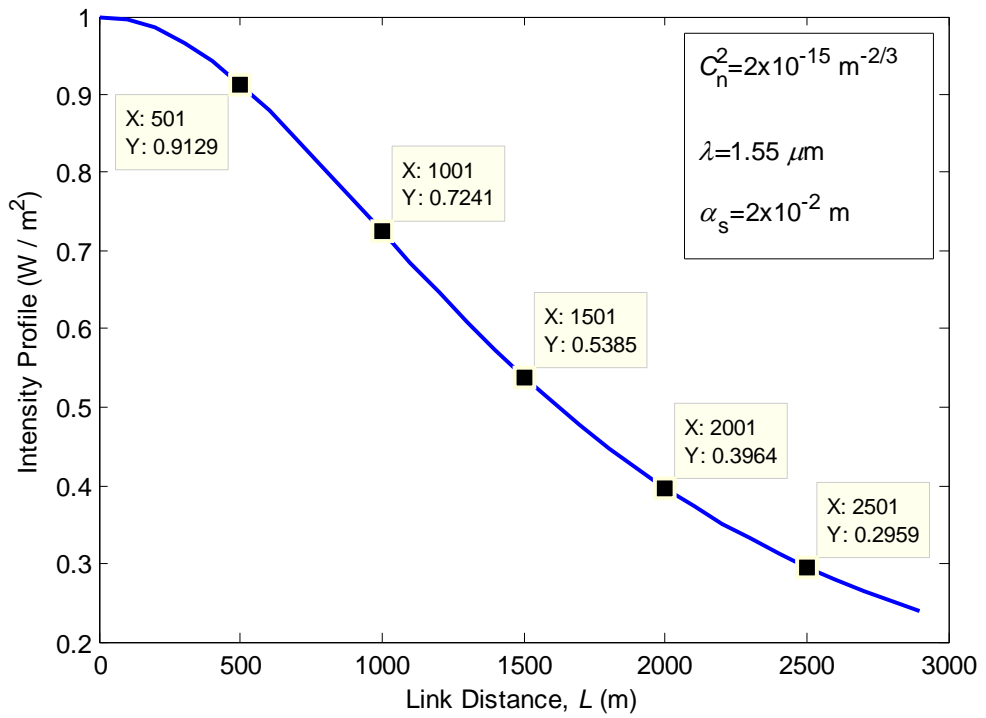


**Figure 3.2** Intensity profile versus the link distance in the atmosphere when the Rytov method is used.

As can be seen in Figure 3.1 and Figure 3.2, the measured data are found to be very close to each other.

### 3.2 Results on the Average Intensity in Underwater Media

In this section, the plots for the intensity profiles of the Gaussian beam propagating in a turbulent underwater medium are given. The plots cover three different link distances. Figure 3.3 is obtained from Equation 2.28.

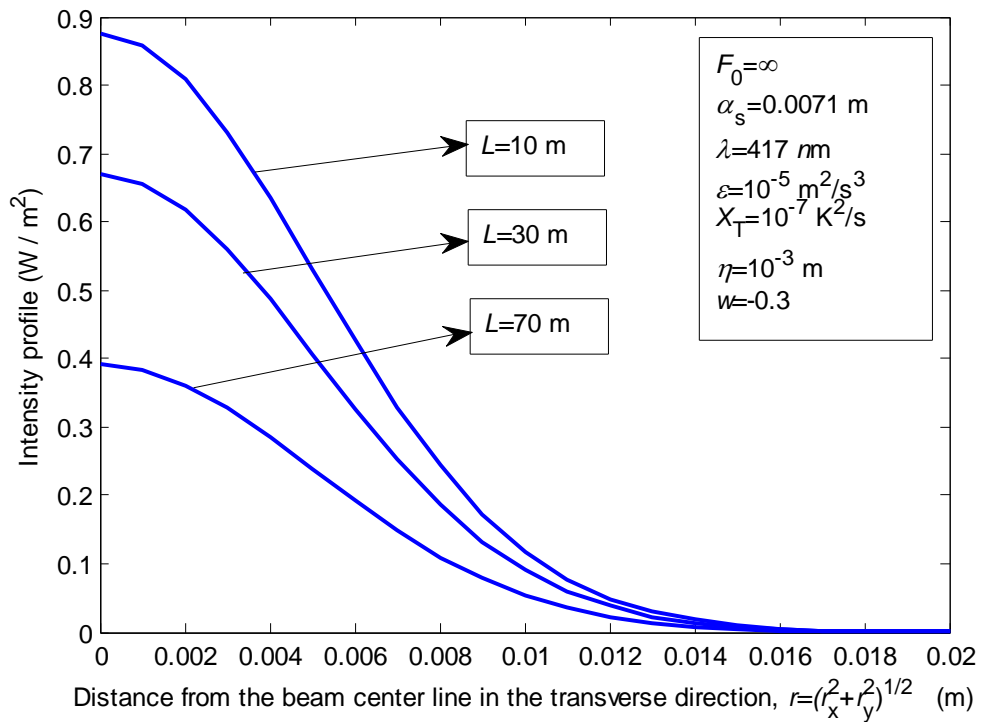


**Figure 3.3** Intensity profile versus distance from beam center line in the transverse direction  $r$  for different link distance  $L$ .

As can be seen in Figure 3.3, the link distance affects the intensity directly. To observe the intensity profile, the values of parameters are taken as  $F_0 = \infty$ ,  $\alpha_s = 0.71$  cm,  $\lambda = 417$  nm,  $\varepsilon = 10^{-5} \text{ m}^2/\text{s}^3$ ,  $X_T = 10^{-7} \text{ K}^2/\text{s}$ ,  $\eta = 10^{-3}$  m and

$w = -0.3$ . These parameters were defined above in chapter 2. This figure and results were compared to Korotkova's result in reference [18]. Such comparison provided satisfactory results. Though there are some differences for  $L=10$  m and  $L=70$  m, the curve of  $L=30$  m is nearly the same. Moreover, characteristics of the curves show the same behaviors.

In Figure 3.4, the average intensity profile is plotted for different beam sizes. The values of the parameters are given in Figure 3.4.

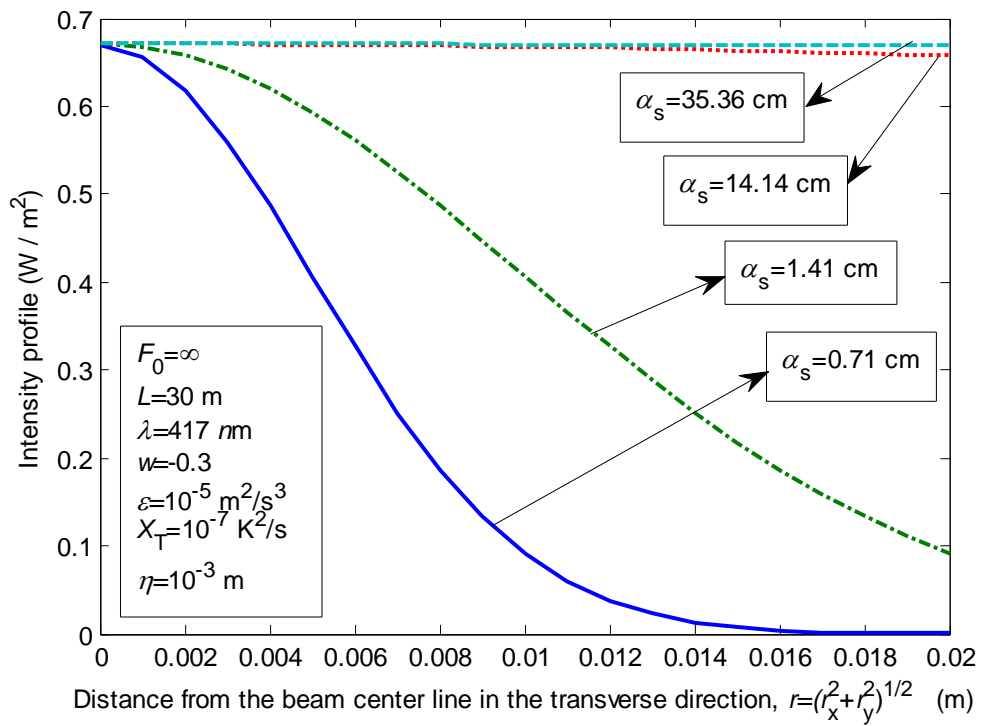


**Figure 3.4** The average intensity profile versus  $r$  for different beam size  $\alpha_s$ .

As can be seen in Figure 3.4, changes in  $\alpha_s$  does not affect the amplitude of intensity for  $r = 0$ . When  $\alpha_s$  is larger, the beam approaches to plane wave form.

### 3.3 Results on the Average Transmittance in Underwater Media

In this section, the average transmittance is analyzed when the Gaussian beam propagates in underwater turbulence. The results are presented mainly by using the average transmittance definition in Equation 2.32, i.e., by using the normalization with respect to the received intensity without turbulence. The results found by using Equation 2.33 are mostly similar to the results obtained by using Equation 2.32 since small link distances are used. For this reason, only a few examples are given by using Equation 2.33. The variations of the average transmittances with respect to the parameters  $w$ ,  $X_T$ ,  $\varepsilon$ ,  $L$ ,  $\lambda$ , and  $\eta$  are evaluated. Sample code prepared in Matlab is given in Appendix A. In these graphs, if not mentioned otherwise, the values of the parameters are taken to be  $w = -0.3$ ,  $X_T = 10^{-7} \text{ K}^2/s$ ,  $\varepsilon = 10^{-5} \text{ m}^2/s^3$ ,  $L = 30 \text{ m}$ ,  $\lambda = 417 \text{ nm}$ ,  $\eta = 10^{-3} \text{ m}$ . Temperature and salinity contributions that are represented by  $w$  affect the turbulence and thus the transmittance, significantly. First set of figures are for the variation of the average transmittance versus  $w$  for different  $X_T$ ,  $\varepsilon$ ,  $L$ , and  $\lambda$ .

The variation of the average transmittance is observed against the ratio of the salinity to temperature contributions  $w$  for different  $X_T$  values in Figure 3.5. In ocean waters,  $w$  takes the value within the interval  $[-5, 0]$ . -5 defines the temperature-induced optical turbulence, 0 determines the salinity-induced oceanic turbulence. As seen in Figure 3.5, the temperature-induced optical turbulence ( $w=-5$ ) has almost no effect on the average transmittance. However, the salinity-induced optical turbulence makes the average transmittance nearly zero especially in the interval  $[-0.5, 0]$  for all

the  $X_T$  values. Salinity-induced oceanic turbulence increases dramatically in between  $w = -0.3$  and  $w = 0$  whatever the value of the rate of dissipation of the mean-squared temperature is. If  $X_T$  is smaller, the average transmittance is affected less from the salinity-induced oceanic turbulence.

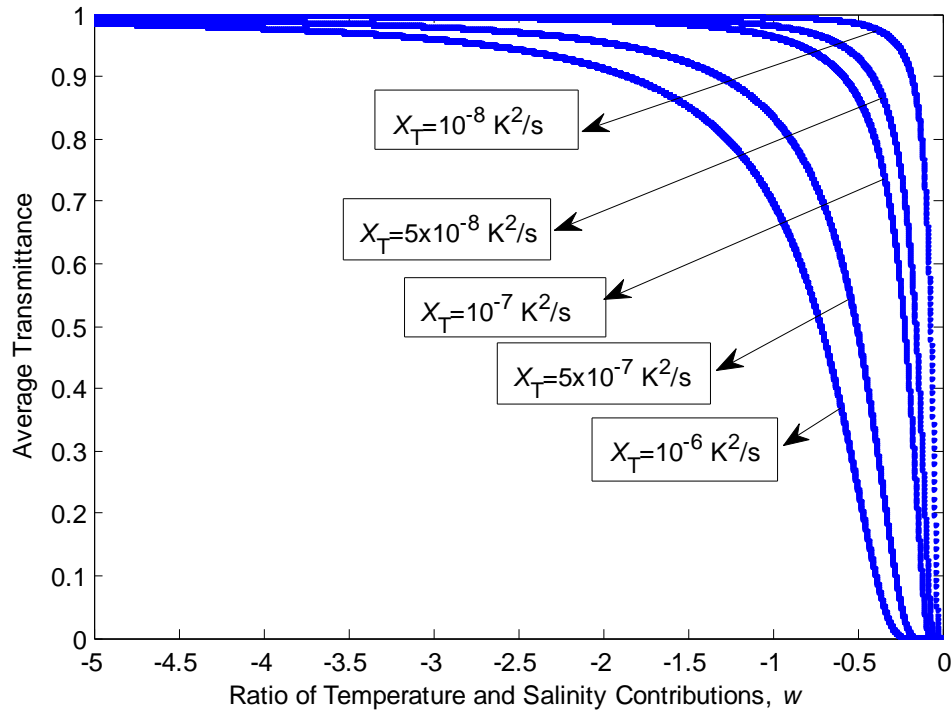


**Figure 3.5** The average transmittance versus the ratio of the salinity-temperature contributions for different  $X_T$  values.

The graphs of the average transmittance versus  $w$  are presented in Figure 3.6 for different values of the rate of dissipation of kinetic energy per unit mass of fluid. For high values of  $\varepsilon$ , the average transmittance stays almost constant until a certain  $w$  value. For example when  $\varepsilon$  equals to  $10^{-1} \text{ m}^2/\text{s}^3$ , the corresponding curve goes straight until  $w = -0.5$ . After that point a sharp decrease is observed. When  $\varepsilon$  is decreased, the average transmittance values decrease more gradually with respect to

$w$ . Additionally, when  $w$  is close to -5 (salinity-induced oceanic turbulence), the average transmittance starts to diminish at a smaller  $w$ .

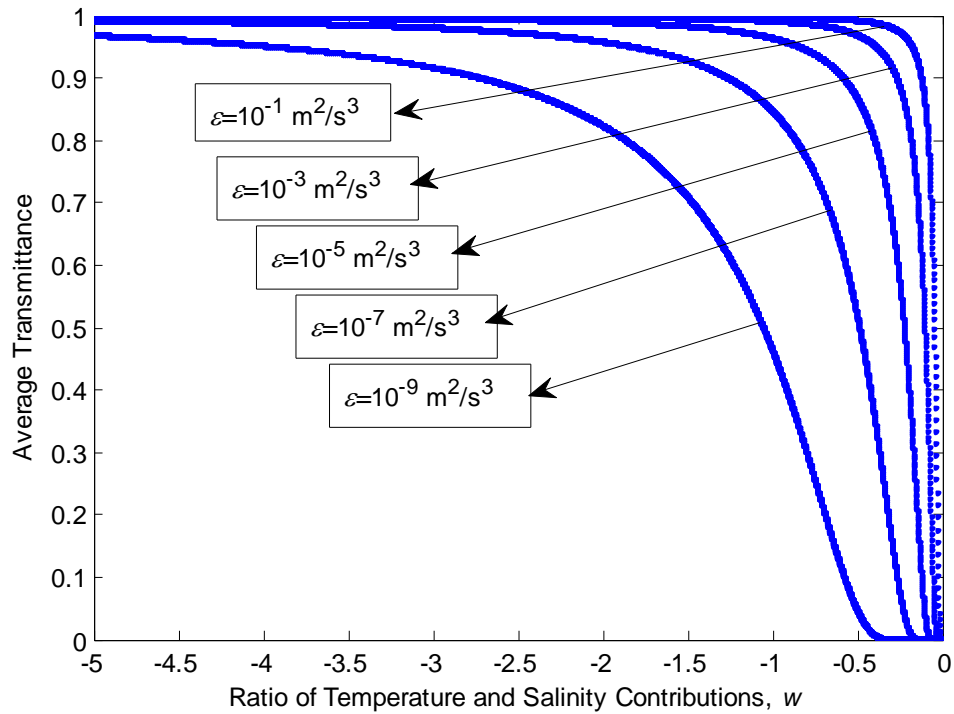


**Figure 3.6** The average transmittance versus the ratio of the salinity-temperature contributions for different  $\varepsilon$  values.

In Figure 3.7, the average transmittance versus  $w$  is examined for various link distances. For five different link distance values, the trends of the average transmittance versus  $w$  characteristics are similar to each other. At a fixed  $w$ , the average transmittance is smaller for longer link distances.

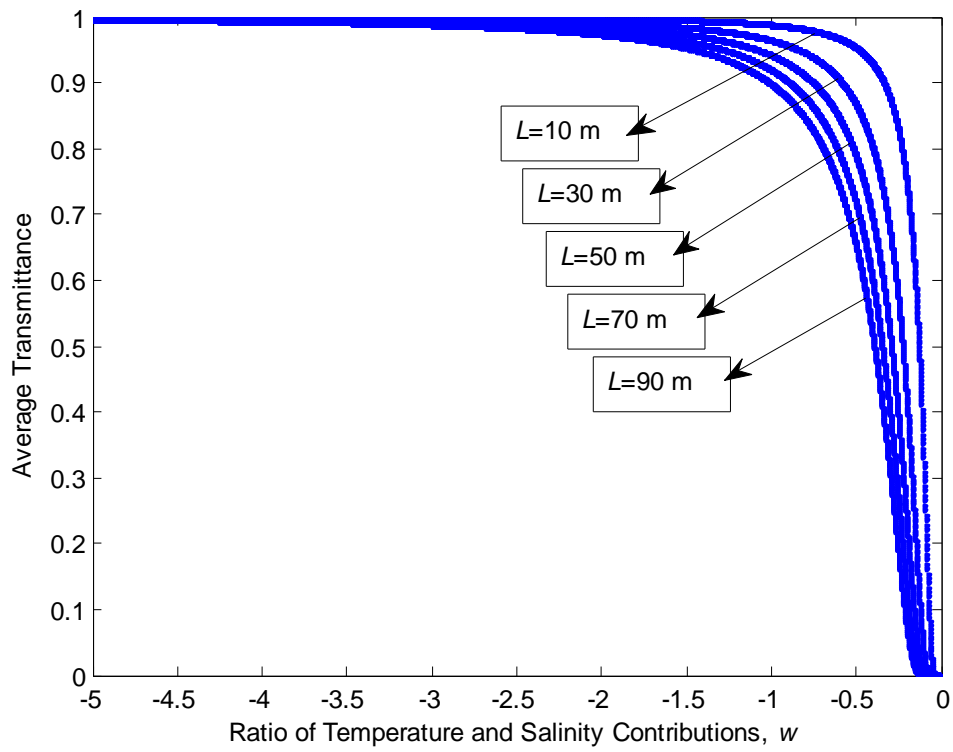


**Figure 3.7** The average transmittance versus the ratio of the salinity-temperature contributions for different  $L$  values.

In Figure 3.8, the decrease in the average transmittance as  $w$  increases is seen for all the wavelengths. Significant decrease in the average transmittance is observed when salinity contribution becomes very high. At a fixed  $w$ , the average transmittance becomes lower at shorter wavelengths.

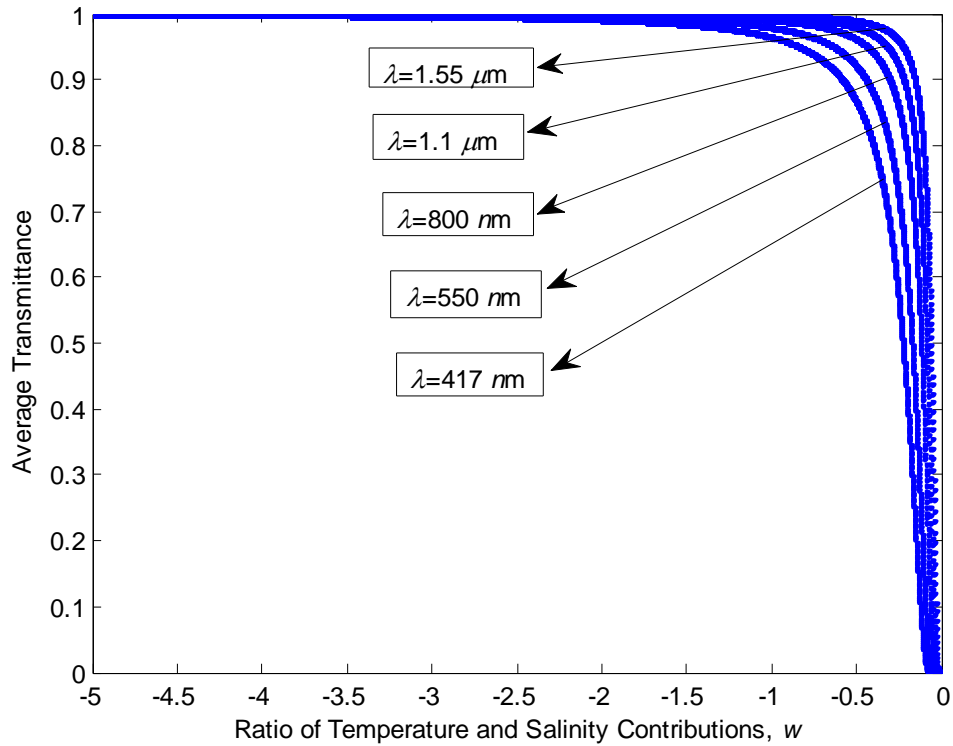


**Figure 3.8** The average transmittance versus the ratio of the salinity-temperature contributions for different  $\lambda$  values.

$X_T$  is one of the other important parameters occurring in the turbulent ocean. The average transmittance versus  $X_T$  variations are examined for different  $\varepsilon$ ,  $L$ , and  $\lambda$  values.

The range of  $X_T$  is usually from  $10^{-4} \frac{\text{K}^2}{\text{s}}$  to  $10^{-10} \frac{\text{K}^2}{\text{s}}$ . The lower bound

$10^{-10} \frac{\text{K}^2}{\text{s}}$  substitutes for no turbulent medium. The upper bound of  $X_T$  means strong turbulence. From Figure 3.9, it is seen that the average transmittance decreases when  $X_T$  becomes larger which is valid for all  $\varepsilon$ . In other words, the average transmittance is less attenuated at low values of the rate of dissipation of



turbulent kinetic energy. When  $X_T$  is fixed, the average transmittance is smaller for smaller  $\varepsilon$  values.

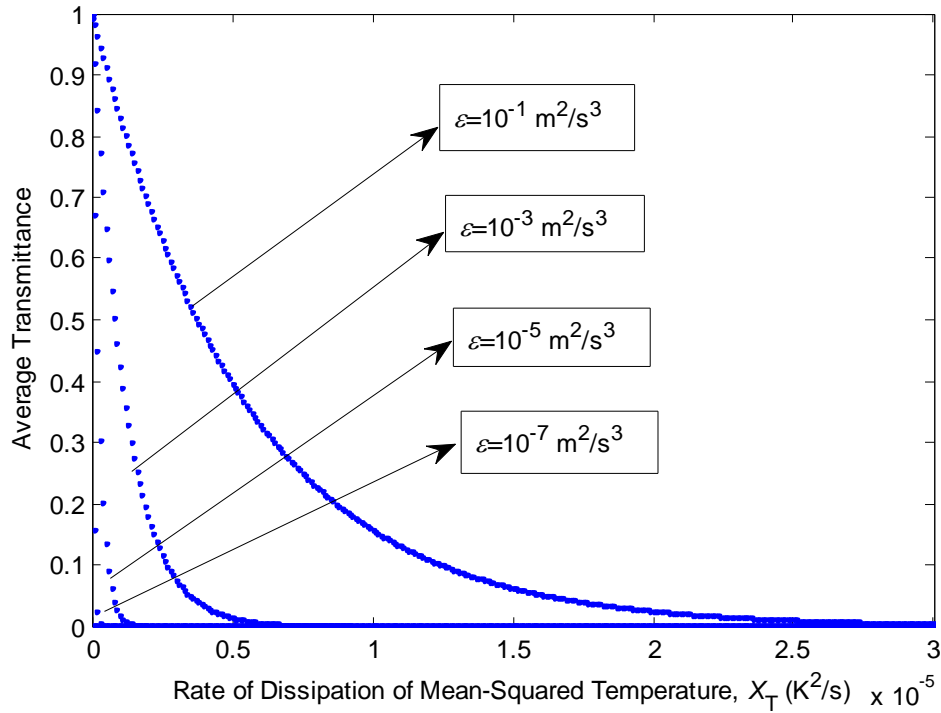


**Figure 3.9** The average transmittance versus the rate of dissipation of the mean-squared temperature for different  $\varepsilon$  values.

In Figure 3.10, the average transmittances are shown versus the rate of dissipation of the mean-squared temperature for different link distances. For all  $L$  values, the behaviour of the curves is similar. For a fixed  $X_T$ , at short link distances, the attenuation in the average transmittance is less as expected.

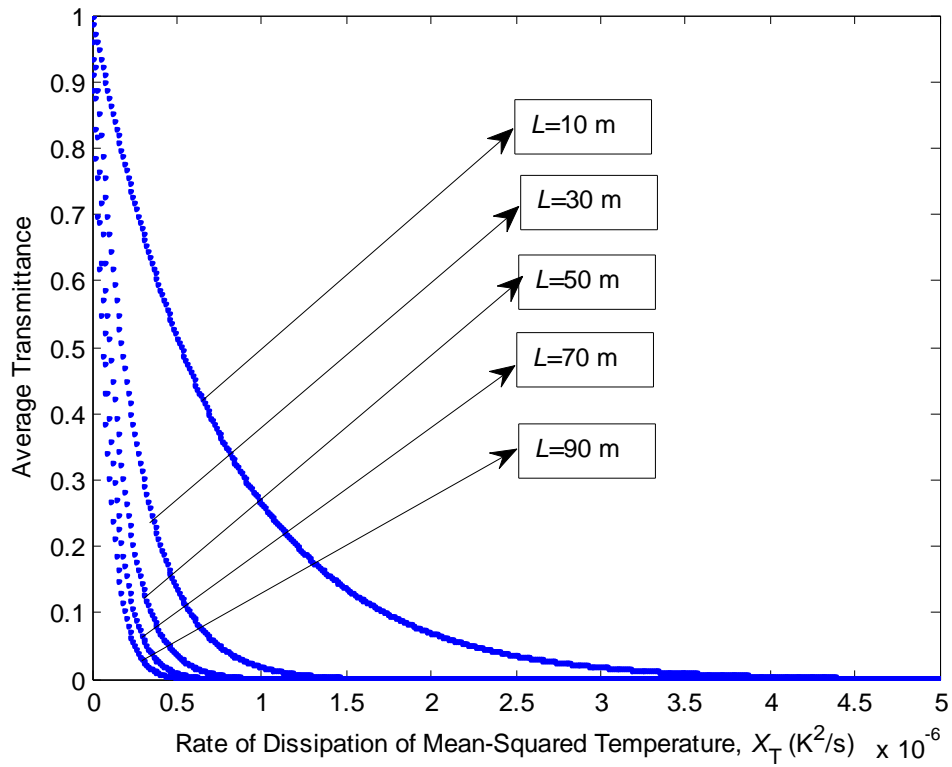


**Figure 3.10** The average transmittance versus the rate of dissipation of the mean-squared temperature for different  $L$  values.

In Figure 3.11, the relation between the average transmittance and the rate of dissipation of the mean-squared temperature  $X_T$  is examined for different wavelengths. As  $X_T$  increases, the average transmittance seems to decrease for all the wavelengths. As the wavelength decreases, the average transmittance becomes smaller at a fixed  $X_T$ .

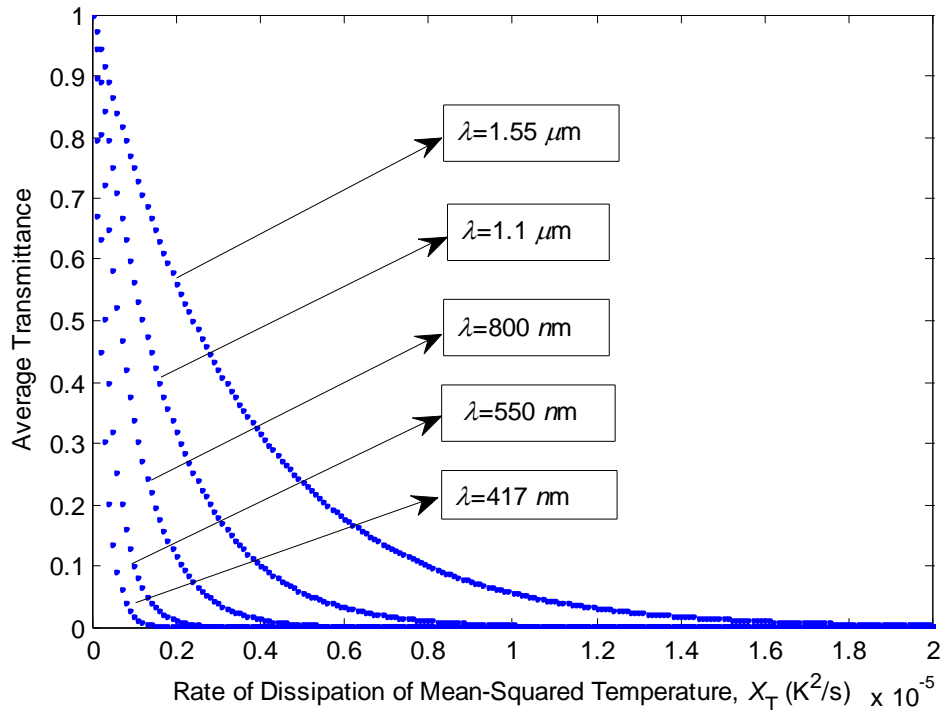


**Figure 3.11** The average transmittance versus the rate of the dissipation of the mean-squared temperature for different  $\lambda$  values.

To observe the average transmittance versus the link distance for different  $\varepsilon$  and  $\lambda$ , Figure 3.12 and 3.13 are provided. From Figure 3.12, it is seen as expected that as the link distance increases, the average transmittance decreases for all  $\varepsilon$ . Smaller  $\varepsilon$  yields smaller average transmittance value at the same link distance.

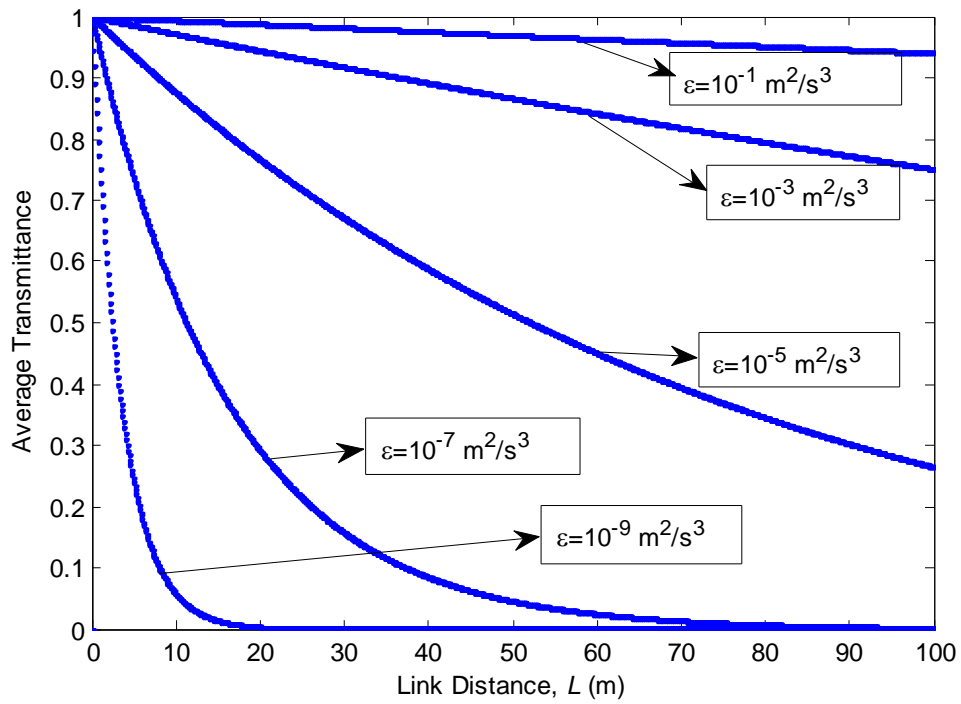


**Figure 3.12** The average transmittance versus the link distance for different  $\epsilon$  values.

In Figure 3.13, in the blue-green region of the wavelength spectrum, the average transmittance exhibits window which is not the case for the longer wavelengths. It is seen that the average transmittance decreases more at small wavelengths.

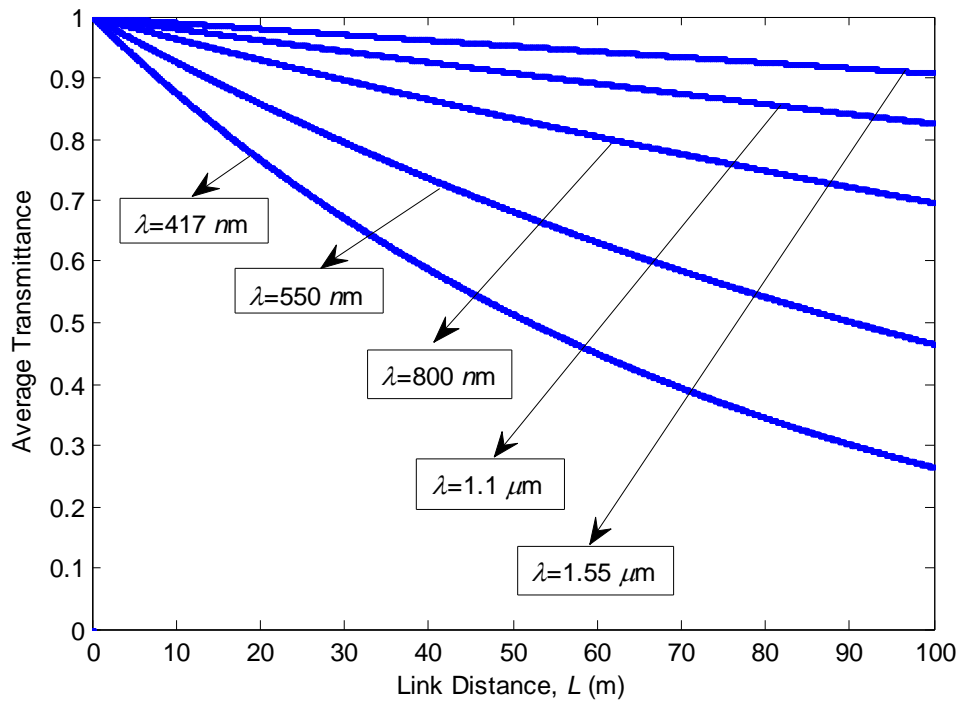


**Figure 3.13** The average transmittance versus the link distance for different  $\lambda$  values.

In Figure 3.14 the average transmittance versus the wavelength is plotted for various  $\varepsilon$  values. As seen in Figure 3.14, a decrease in the average transmittance can be observed when the wavelength becomes shorter. For the same wavelength, larger  $\varepsilon$  gives larger average transmittance values.

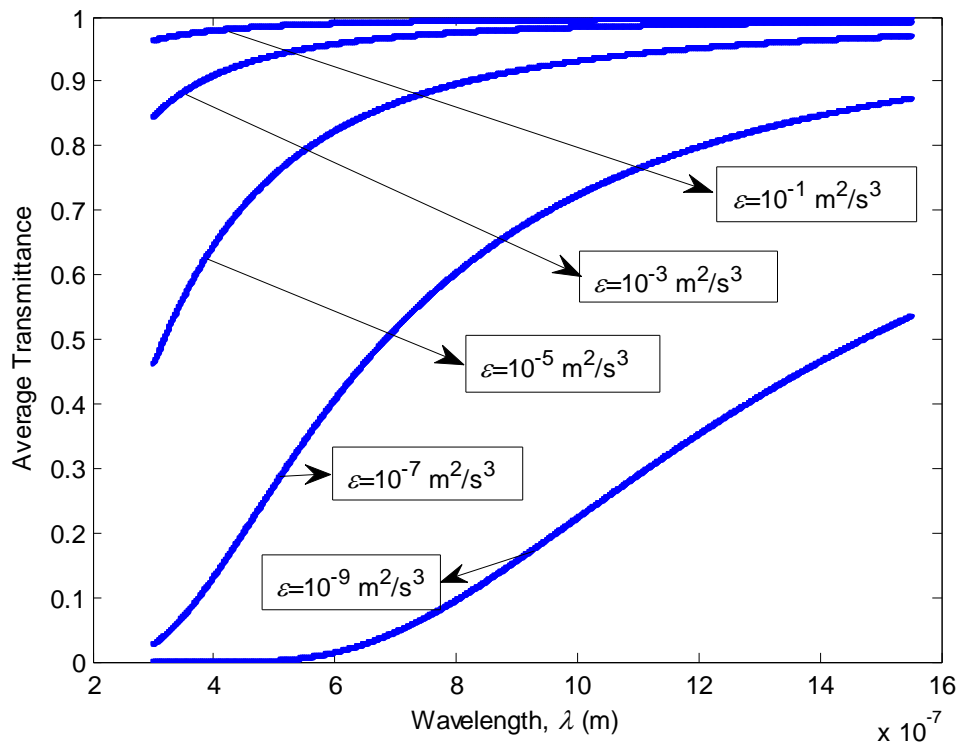


**Figure 3.14** The average transmittance versus the wavelength for different  $\epsilon$  values.

In Figures 3.15 to 3.19, the effect of the Kolmogorov microscale length (inner size)  $\eta$  on the average transmittance is observed for various parameters such as  $w$ ,  $X_T$ ,  $\epsilon$ ,  $L$  and  $\lambda$ . In these figures, the microscale length is defined in the range from  $10^{-3}$  m to  $10^{-2}$  m.

For Figure 3.15, when the microscale length is about  $7.5 \times 10^{-3}$  m and bigger than this value, for all  $w$ , the average transmittance takes the constant value which is nearly one. After this value, the effect of  $\eta$  on the average transmittance cannot be observed no matter what value  $w$  takes. However, before this value, the salinity-induced ( $w$  being around 0) and temperature-induced ( $w$  is about -5) optical

turbulence effect on the average transmittance can be observed. When the value of the  $w$  is less than -2, the average transmittance almost stays fixed for any  $\eta$ . At a fixed  $\eta$ , larger  $w$  yields smaller average transmittance.

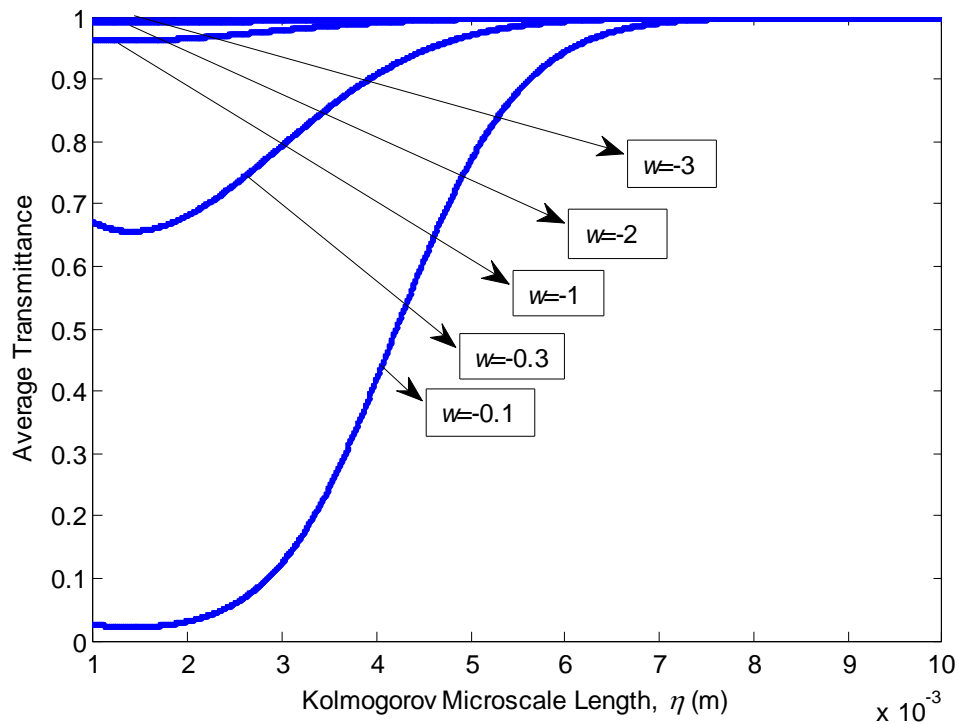


**Figure 3.15** The average transmittance versus Kolmogorov microscale length for different  $w$  values.

In Figure 3.16, curves of the average transmittance versus  $\eta$  are plotted for different  $X_T$  values in the defined range. For any  $X_T$ , the decrease on the average transmittance is not seen when  $\eta$  takes values above  $7.5 \times 10^{-3}$  m. It is concluded that at fixed  $\eta$ , the average transmittance becomes smaller for larger  $X_T$ .

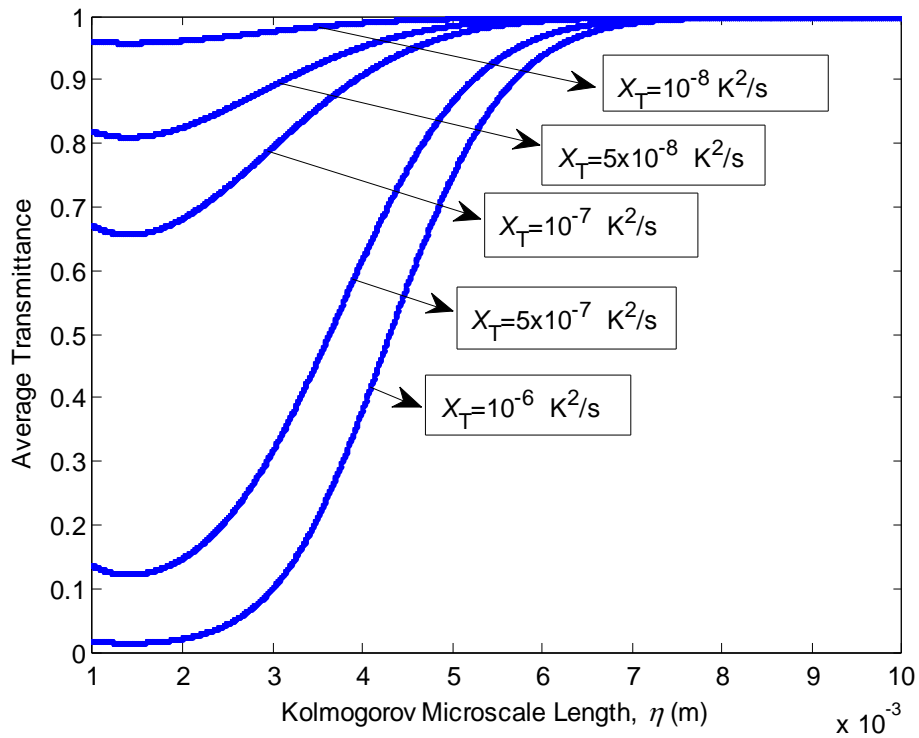


**Figure 3.16** The average transmittance versus Kolmogorov microscale length for different  $X_T$  values.

Examining the average transmittance variations against  $\eta$  for different  $\varepsilon$  values in Figure 3.17, it is seen that for all  $\varepsilon$  values, when the microscale length is larger than  $7.5 \times 10^{-3}$  m, the variation in the average transmittance is not observed and the average transmittance attains unity value. Larger  $\varepsilon$  values cause the average transmittance to take smaller values when the microscale length stays at a fixed value.



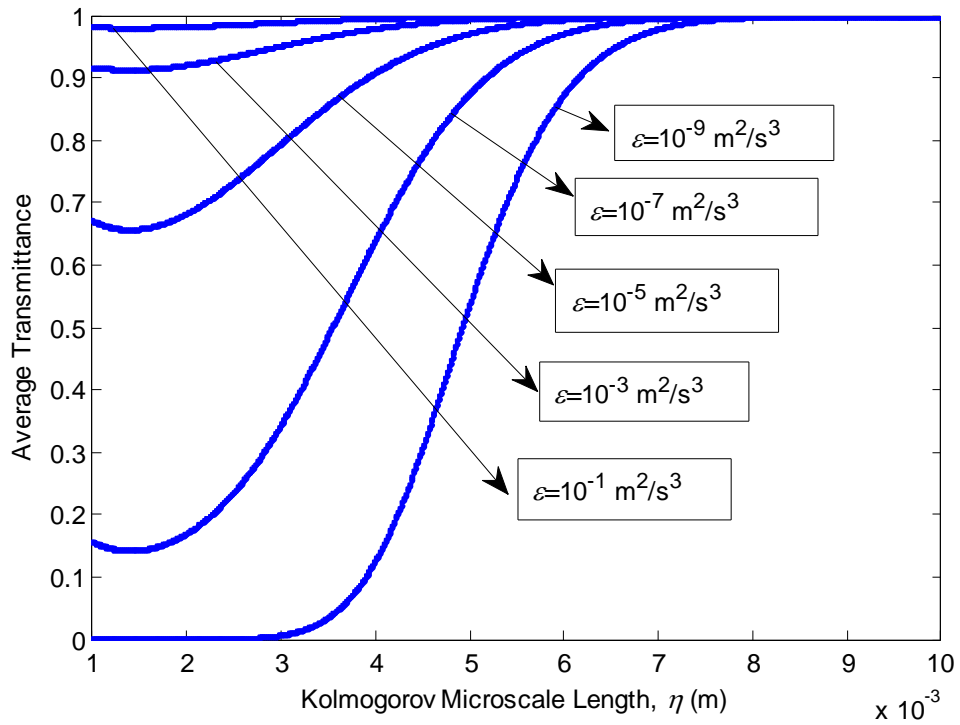


**Figure 3.17** The average transmittance versus Kolmogorov microscale length for different  $\epsilon$  values.

In Figure 3.18, the change in the average transmittance with respect to Kolmogorov microscale is analysed for different link distances. As the microscale length increases, the average transmittance is increased in general. When  $\eta$  is larger than  $7 \times 10^{-3}$  m, the average transmittance stays at unity no matter what link distance is considered. For fixed  $\eta$ , large link distances cause the average transmittance to attain smaller values.

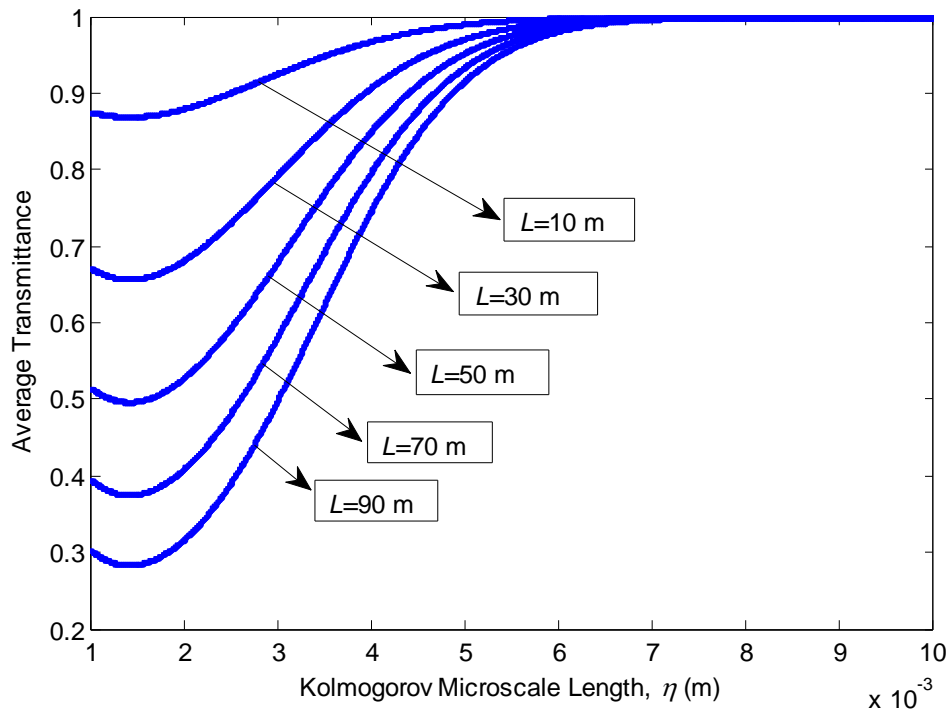


**Figure 3.18** The average transmittance versus Kolmogorov microscale length for different  $L$  values.

The graphs of the average transmittance versus Kolmogorov microscale are provided in Figure 3.19 which indicates that the average transmittance increases as the microscale length increases at any wavelength. This increase in the average transmittance continues until when  $\eta$  reaches a value around  $7 \times 10^{-3}$  m. After this value of  $\eta$ , the average transmittance seems to stay at a fixed value of unity for any wavelength. Shorter wavelengths exhibit smaller average transmittances when the microscale is constant.

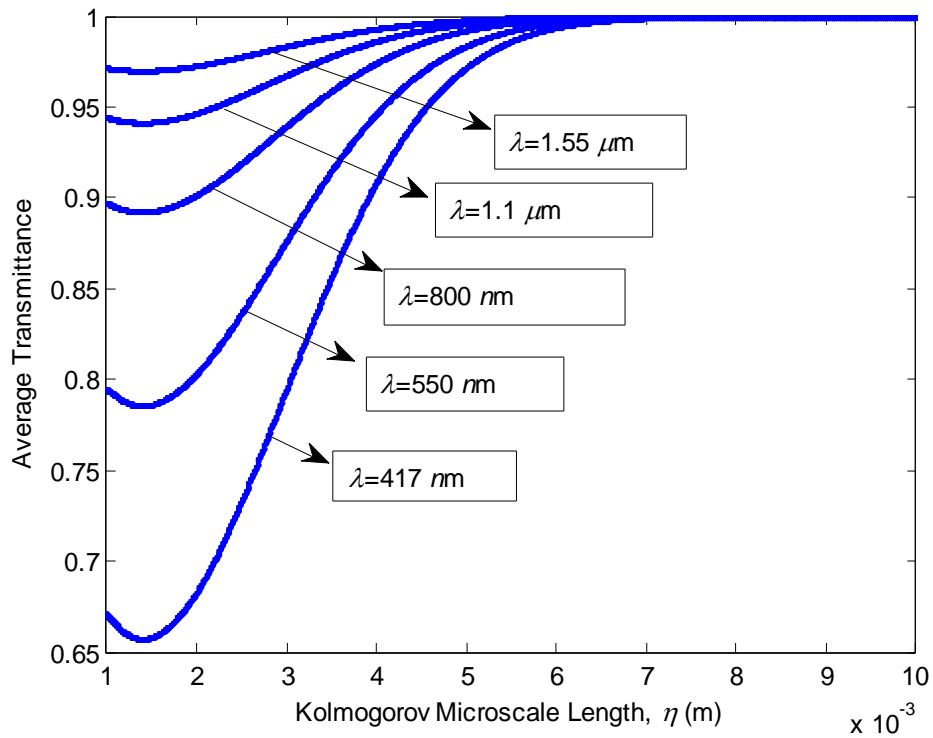


**Figure 3.19** Average transmittance versus Kolmogorov microscale length for different  $\lambda$  values.

As also mentioned above, in this work, the results on the average transmittance are obtained by using Equation 2.32 which defines the average transmittance as the average received intensity in turbulence normalized by the received intensity in the absence of turbulence. In this thesis work, the results for the average transmittance using the definition provided by Equation 2.33 are also taken. However, these results, which are not presented in this thesis are quite similar to the results obtained by using Equation 2.32, mainly because of the small link distances employed in our evaluations our findings are at the receiver origin, i.e., at  $r = 0$ .

We have also searched for the effect of the source size  $\alpha_s$  on the average transmittance but no distinct effect of  $\alpha_s$  is found which is again attributed to the fact

that our evaluations involve small link distances and the calculations are made at the receiver origin.

## CHAPTER 4

### CONCLUSION

#### 4.1 Conclusion

In this thesis, the effect of oceanic turbulence on the average transmittance is analyzed for the lowest order collimated Gaussian beam source. Used power spectrum to constitute the oceanic turbulence was assumed for homogeneous and isotropic oceanic water with the eddy thermal diffusivity and diffusion of salt. Changing the parameters of power spectrum and the parameters of the beam, the average transmittance is analyzed. Received field in underwater turbulence is calculated by Rytov method using numerical integration. To ensure the correctness of the results, certain checks are performed. For atmospheric turbulence check, the average intensity is calculated both by employing the extended Huygens-Fresnel integral with analytic integration and the Rytov method with numerical integration. Then, for the oceanic turbulence, again the average intensity is calculated using our method and the results are compared with Korotkova's [18] results. In our evaluations of the average transmittance, all of the important parameters which constitute the oceanic turbulence such as the ratio of the temperature and salinity contributions to the refractive index spectrum  $w$ , the rate of dissipation of kinetic energy per unit mass of fluid  $\varepsilon$ , the rate of dissipation of the mean-squared

temperature  $X_T$ , and the Kolmogorov micro scale length (inner scale)  $\eta$  are examined. Moreover, the effects of the link distance  $L$  and the wavelength  $\lambda$  on the average transmittance are examined.

Examining the effect of the ratio of the temperature and salinity contributions to the refractive index spectrum on the average transmittance, it is observed that the temperature-induced optical turbulence has almost no attenuation effects on the average transmittance, however, the salinity-induced optical turbulence reduces the transmittance suddenly for certain values of  $w$ . For the small value of the rate of dissipation of kinetic energy per unit mass of fluid  $\varepsilon$ , the average transmittance is lower as compared to the average transmittance obtained at the larger values of  $\varepsilon$ . When different values of  $\varepsilon$  are analyzed with changing values of other variables, high turbulence effect is observed for small values of  $\varepsilon$ . If the dissipation rate of the kinetic energy has higher value, the turbulence effect decreases and thus the average transmittance increases. The rate of dissipation of mean-squared temperature  $X_T$  is inversely proportional to the average transmittance. When the dissipation rate of the mean-squared temperature increases, turbulence effect increases, so the average transmittance decreases. Link distance  $L$  has inverse effect on the average transmittance, irrespective of the turbulence parameters of the medium. In this respect, the ocean water forms a limited environment for the propagation of light since even a small  $L$  can be enough to diminish the average transmittance detected at the receiver of an underwater optics communication link. The wavelength is another factor affecting the light propagation directly. Considering only the turbulence effect in an underwater medium, when  $\lambda$  is longer, the average transmittance values

become higher. The Kolmogorov microscale  $\eta$  also affects the average transmittance. Increasing  $\eta$  to a certain value, the average transmittance decreases because of the increasing turbulence effect to this value, however, when  $\eta$  exceeds this value, the average transmittance starts to increase. Further increase in  $\eta$  results in the saturation of the average transmittance at large values. The source size effect is too small when the average transmittance is evaluated on the origin of receiver plane.

## **4.2 Future Works**

In this study, on-axis wave propagation is examined, and the average intensity and the average transmittance are calculated for the Gaussian beam. The formulation and the results presented in this thesis can be expanded to cover the off-axis propagation and for other types of incidences such as the flat-topped, annular and sinusoidal Gaussian. Other futuristic aspects of this thesis are the formulations and the evaluations of the intensity fluctuations and the bit error rate. LED excitation analysis of the average transmittance is also interesting to pursue. In this study, turbulence effects are observed for isotropic and homogeneous ocean water when the eddy thermal diffusivity and diffusion of salt are assumed to be equal. To improve the studied model, different water types can be tried to analyze, so different power spectra can be searched and used. Under appropriate infrastructure, an experimental set up can be established in order to compare the theoretical findings with the experimental outcomes.

## REFERENCES

- [1] **BRUNDAGE, H.** (2010), *Designing a Wireless Underwater Optical Communication System*, a thesis submitted to the Department of Mechanical Engineering of MIT in partial fulfillment of the requirements for the degree of Master of Science in Mechanical Engineering.
- [2] **ARNON, S., KEDAR, D.** (2009), *Non-line-of-sight underwater optical wireless communication network*, J. Opt. Soc. Am., 530-539, Vol. 26, No.3.
- [3] **ARNON, S.** (2010), *Underwater Optical Wireless Communication Network*, Optical Engineering 49(1), 015001.
- [4] **SIMPSON, J.** (2007), *A 1 Mbps Underwater Communications System using LEDs and Photodiodes with Signal Processing Capability*, a thesis submitted to the Graduate Faculty of North Carolina State University in partial fulfillment of the requirements for the degree of Master of Science in Electrical Engineering Raleigh, North Carolina.
- [5] **SMART, J. H.**, *Underwater Optical Communications Systems Part 1: Variability of Water Optical Parameters*, Applied Physics Laboratory of The Johns Hopkins University, Laurel, MD.
- [6] **CONHENOUR, B. M., MULLEN, L. J., LAUX, A. E.** (2008), *Characterization of the beam-spread function for underwater wireless communications links*, IEEE Journal of Oceanic Engineering, 513-521, Vol. 33, No. 4.
- [7] **HANSON, F., RADIC, S.** (2008), *High bandwidth underwater optical communication*, Applied Optics, 277-283, Vol. 47, No. 2.
- [8] **GABRIEL, C., KHALIGHI, M. A., BOURENNANE S., LEON P., RIGAUD, V.**, *Channel Modeling for Underwater Optical Communication*, Institute Fresnel, UMR CNRS 6133, Marseille, France IFREMER, La Mer.



- [9] **LI, J., MA, Y., ZHOU, Q., ZHOU, B., WANG, H.** (2012), *Monte Carlo study on pulse response of underwater optical channel*, *Optical Engineering* 51(6), 066001.
- [10] **MOBLEY, C.** (1994), *Light and Water*, Academic Press/Elsevier Science, San Diego, CA.
- [11] **CHANCEY, M. A.** (2005), *Short range underwater optical communication links*, a thesis submitted to the Graduate Faculty of North Carolina State University in partial fulfillment of the requirements for the degree of Master of Science in Electrical Engineering Raleigh, North Carolina.
- [12] **GAWDI, Y. J.** (2006), *Underwater free space optics*, a thesis submitted to the Graduate Faculty of North Carolina State University in partial fulfillment of the requirements for the degree of Master of Science in Electrical and Computer Engineering Raleigh, North Carolina.
- [13] **SMYTH, W. D., MOUM, J. N.** (2001), *3D Turbulence*, College of Oceanic and Atmospheric Sciences Oregon State University, Academic Press, doi:10.1006/rwos.2001.0134
- [14] **BALES, J., CHRYSOSTOMIDIS, C.** (1995), *High-bandwidth, low-power, short-range optical communication underwater*, 9<sup>th</sup> International Symposium on Unmanned Untethered Submersible Technology.
- [15] **GILES, J. W., BANKMAN, I. N.** (2005), *Underwater Optical Communication Systems Part 2: Basic Design Considerations*, MILCOM.
- [16] **FARR, N., et. al.** (2006), *Optical Modem technology for seafloor observatories*, Proceedings of the IEEE Oceans.
- [17] **SHCHEPAKINA, E., FARWELL, N., KOROTKOVA, O.** (2011), *Spectral changes in stochastic light beams propagating in turbulent ocean*, *Appl. Phys. B.*, DOI 10.1007/s00340-011-4626-9.
- [18] **FARWELL N., KOROTKOVA, O.** (2012), *Intensity and coherence properties of light in oceanic turbulence*, *Optics Communication* 285, 872-875.
- [19] **OKOOMIAN, H. J.** (1966), *Underwater transmission characteristics for laser radiation*, *Applied Optics*, 1441-1446, Vol. 5, No. 9.

- [20] **PIERCE, J. W.**, et. al. (1986), *Response of underwater light transmittance in the Rhode River eustary to changes in water quality parameters*, Estuaries, 169-178, Vol. 9, No. 3.
- [21] **NICOLAUS, M.**, et. al. (2013), *Variability of light transmission through Arctic land-fast ice during spring*, The Cryosphere, 7, 977-986.
- [22] **BAYKAL, Y.** (2004), *Average transmittance in turbulence for partially coherent sources*, Optics Communication 231, 129-136.
- [23] **ATA, Y., BAYKAL, Y.** (2011), *Turbulence effect on transmittance of atmospheric optics telecommunication system using dense wavelength division multiplexing*, Journal of Modern Optics, 1644-1650, Vol. 58, No. 18.
- [24] **SALEH, B. E. A., TEICH, M., C.** (2007), *Fundamentals of Photonics*, John Wiley, Sons, Inc, Hoboken, New Jersey, Canada.
- [25] **ANDREWS, R. C., PHILLIPS, R. L.** (1998), *Laser Beam Propagation through Random Media*, The International Society for Optical Engineering, Bellingham, Washinton.
- [26] **ANDREWS, L. C.** (1998), *Special functions of Mathematics for Engineers*, The International Society for Optical Engineering, Bellingham, Washington.
- [27] **NIKISHOV, V. V., NIKISHOV V. I.** (2000), *Spectrum of turbulent fluctuation of the sea water refractive index*, International Journal of Fluid Mechanics Research, 27, 82-98.
- [28] **SERMUTLU, E.** (2010), *Numerically evaluates double integrals over rectangular regions using 64, or 48, or 32, or 24-point Gaussian Rule* (unpublished), Matlab code, Çankaya University, Ankara.
- [29] **GÖKÇE, M. C.** (2012), *Scintillation analysis and evaluation of Super Lorentz-Gaussian laser beams for optical wireless*, Master thesis for Ankara University, Graduate School of Natural Applied Science, departmans of Electronics Engineering.
- [30] **KAMACIOĞLU, C., BAYKAL, Y., YAZGAN E.** (2012), *Düz tepeli ışık hüzmelerinin türbülanslı atmosferde yayılımında alıcı açıklığı etkileri*, 6. URSI Konferansı, Doğu Üniversitesi, İstanbul.

- [31] **ANDREWS, L. C.** (2004), *Field guide to atmospheric optics*, The International Society for Optical Engineering, Bellingham, Washington.

## APPENDIX A

### SAMPLE MATLAB CODE

```
% _____ AVERAGE TRANSMITTANCE VERSUS w GRAPH _____ %  
% _____ for different Xt values _____ %  
% _____ %  
  
clc; clear all; close all;  
wl=0.417e-6; % wavelength (default value)  
  
%wl=[0.417e-6 0.55e-6 0.8e-6 1.1e-6 1.55e-6]; %wavelength (to  
observe the average transmittance for different values)  
  
%wl=0.38e-6:1e-9:1.55e-6; %wavelength (to observe the changes on  
average transmittance according to wavelength)  
  
k=2*pi./wl; %wave number  
  
L=30; % link distance (default value)  
  
%L=[10 30 50 70 90]; %link distance (to observe the average  
transmittance for different values)  
  
%L=0:0.1:100; %link distance (to observe the average transmittance  
according to link distance)  
  
epsilon=1e-5; %rate of dissipation of kinetic energy per unit mass  
of fluid (default value)  
  
%epsilon=[1e-1 1e-3 1e-5 1e-7 1e-9]; %to observe for different value  
  
%epsilon=1e-10:1e-4:1e-1; % when it is x_axis  
  
%Xt=1e-7; %rate of dissipation of mean-squared temperature (default  
value)  
  
Xt=[1e-6 5e-7 1e-7 5e-8 1e-8]; %to observe for different value  
  
%Xt=1e-10:1e-7:1e-4; % when it is using for x_axis  
  
eta=1e-3; % kolmogorov microscale(inner scale) (default value)  
  
%eta=[1e-2 5e-3 1e-3 1e-4]; % to observe the aveage transmittance  
for diferent value
```

```

%eta=1e-3:1e-5:1e-2; % when it is using x_axis

At=1.8631e-2;
As=1.9e-4;
Ats=9.41e-3;

%w=-0.3; %temperature and salinity contributions to refractive index
spectrum

%w=[-3 -2 -1 -0.3 -0.1]; %temperature to salinity contributions [-
5 0] -5 temp.;0 salinity

w=-5:0.01:0; %to use for x_axis

Wo=0.01; %initial beam size (it is equal to sqrt(2)*alfa_s)
Fo=inf; %phase front radius of curvature determines the collimated
beam

r=0;p=r-r; %position vectors at receiver plane

for a=1:1:length(w);for aa=1:1:length(Xt);
coef=((0.388)*1e-8*(epsilon^(-1/3)))*(Xt(aa)/(w(a)^2));
%%%%%%%%%%%%%%%%%%%%%%%%%%%%%%%%%%%%%%%%%%%%%%%%%%%%%%%%%%%%%%%%%%%%%%%%
tetha_zero=1-L/Fo; % input plane beam parameters
lamda_zero=2*L/k*Wo^2; %input plane beam parameters
lamda=lamda_zero/lamda_zero^2+tetha_zero^2; %output plane beam
parameters
tetha=tetha_zero/lamda_zero^2+tetha_zero^2; %output plane beam
parameters
tetha_dash=1-tetha;
%%%%%%%%%%%%%%%%%%%%%%%%%%%%%%%%%%%%%%%%%%%%%%%%%%%%%%%%%%%%%%%%%%%%%%%%
z=@(K,P)K.*coef.*(K.^(-11/3))...
.*(1+(2.35).*(K.*eta).^(2/3)).*(w(a).^2)...
.*exp(-At.*(8.284).*(K.*eta)...
.^(4/3))+((12.978)*(K.*eta).^2))...
+(exp(-As.*(8.284).*(K.*eta)...
.^(4/3))+((12.978)*(K.*eta).^2))...
-(2.*w(a).*exp(-Ats.*(8.284).*(K.*eta).^(4/3))...
+((12.978)*(K.*eta).^2)))...
.*(1-exp(-lamda.*L.*K.^2.*P.^2/k)...
.*besselj(0,K.*(1-tetha_dash.*P).*p-2*i*lamda.*P.*r));

lo= 2.8560e-007; %inner scale to determine the upper limit of Kappa
Lo= 78.5398; %outher scale to determine the lower limit of Kappa
alt=(2*pi)/Lo; %lower limit of Kappa
ust=(2*pi/lo); %upper limit of Kappa
integ_part=dblquad04(z,alt,ust,0,1,'enson'); %numeric integral
mcf_1(a)=exp(-4*(pi^2).*(k^2)*L*integ_part); %part of adding
turbulence effect

%%%%%%%%%%%%%%%%%%%%%%%%%%%%%%%%%%%%%%%%%%%%%%%%%%%%%%%%%%%%%%%%%%%%%%%%

```

```

alfa=(2/(k.*Wo.^2))+i*(1/Fo); %complex parameter to the spot size
and phase front radius of curvature

Uo=(1./(1+i*L*alfa))*exp((i*k*L)+((i*k)./(2*L))...
.*(i*alfa*L)/(1+i*L*alfa)).*r.^2;% received field without
turbulence

%corelation function mcf
mcf=Uo.*conj(Uo).*mcf_1(a); %turbulent received field (determines
the intensity because of on-axis propagation)
transmittance=mcf/(Uo.*conj(Uo)); %transmittance
plot(w(a),transmittance)
hold on
end
end

title('Average Tranmittance vs Ratio of Temperature and Salinity
Contributions for Different \itX\rm T Values');
xlabel('Ratio of Temperature and Salinity Contributions, \itw');
ylabel('Average Transmittance');

```

## APPENDIX B

### CURRICULUM VITAE

#### PERSONAL INFORMATION

Surname, Name: Keskin, Aysan

Nationality: Turkish (TC)

Date and Place of Birth: 4 February 1986 , Ankara

Marital Status: Single

Phone: +90 505 587 71 20

email: [aysankeskin@gmail.com](mailto:aysankeskin@gmail.com)

#### EDUCATION

Degree	Institution	Year of Graduation
MS	Çankaya Univ.Electronic and Communication Engineering	2013
BS	Çankaya Univ.Electronic and Communication Engineering	2010
High School	Süleyman Demirel Anatolian High School, Ankara	2004

#### FOREIGN LANGUAGE

Advanced English

#### PUBLICATION

Keskin, A., Çatmakaş, Ö. K., Arpalı, S. A., Arpalı, Ç., Eyyuboğlu H. T. (2010), “Kule vinç motorlarında arıza tespit sistemi”, Çankaya Üniversitesi 3. Mühendislik ve Teknoloji Sempozyumu, Ankara, Türkiye, Apr. 2010. Çankaya Üniversitesi 3. Mühendislik ve Teknoloji Sempozyumu Kitapçığı, 421-424, 29-30 Nisan 2010.

